AD-A150 038 AN ITERATION METHOD FOR COMPLEX SCATTERING PROBLEMS(U) 1/1
DAYTON UNIV OH RESEARCH INST M KAYE ET AL. OCT 84
UDR-TR-81 RADC-TR-84-204 F19628-83-K-0034

UNCLASSIFIED F/G 20/6 NL

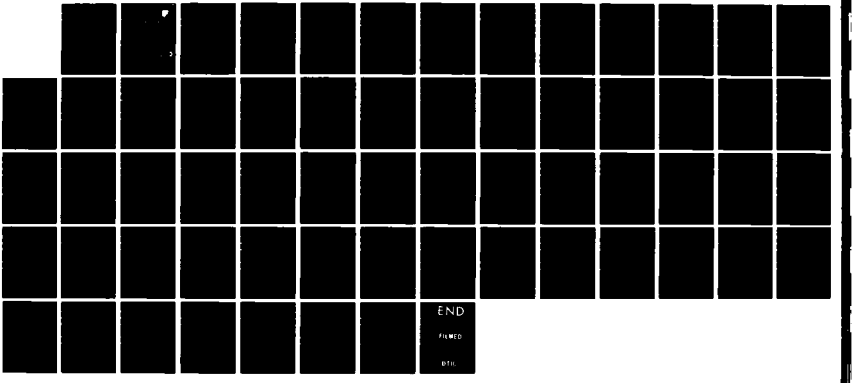

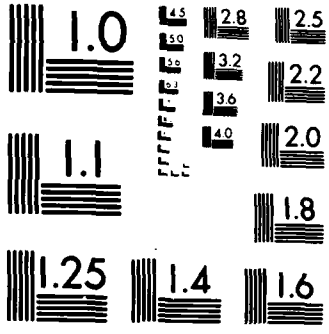

MICROCOPY RESOLUTION TEST CHART
NATIONAL BUREAU OF STANDARDS-1963-A

RADC-TR-84-204
Interim Report
October 1984

AN ITERATION METHOD FOR COMPLEX SCATTERING PROBLEMS

University of Dayton

Michael Kaye
P. Krishna Murthy
Gary A. Thiele

ROME AIR DEVELOPMENT CENTER
Air Force Systems Command
Griffiss Air Force Base, NY 13441-5700

This report has been reviewed by the RADC Public Affairs Office (PA) and is releasable to the National Technical Information Service (NTIS). At NTIS it will be releasable to the general public, including foreign nations.

RADC-TR-84-204 has been reviewed and is approved for publication.

APPROVED: Robert V. McGahan

ROBERT V. McGAHAN
Project Engineer

APPROVED: Allan C. Schell

ALLAN C. SCHELL
Chief, Electromagnetic Sciences Division

FOR THE COMMANDER: John A. Ritz

JOHN A. RITZ
Acting Chief, Plans Office

If your address has changed or if you wish to be removed from the RADC mailing list, or if the addressee is no longer employed by your organization, please notify RADC (EECT) Hanscom AFB MA 01731. This will assist us in maintaining a current mailing list.

Do not return copies of this report unless contractual obligations or notices on a specific document requires that it be returned.

UNCLASSIFIED
SECURITY CLASSIFICATION OF THIS PAGE

REPORT DOCUMENTATION PAGE

1a. REPORT SECURITY CLASSIFICATION UNCLASSIFIED	1b. RESTRICTIVE MARKINGS N/A
2a. SECURITY CLASSIFICATION AUTHORITY N/A	3. DISTRIBUTION/AVAILABILITY OF REPORT Approved for public release; distribution unlimited
2b. DECLASSIFICATION/DOWNGRADING SCHEDULE N/A	
4. PERFORMING ORGANIZATION REPORT NUMBER(S) UDR-TR-84-81	5. MONITORING ORGANIZATION REPORT NUMBER(S) RADC-TR-84-204
6a. NAME OF PERFORMING ORGANIZATION University of Dayton 6b. OFFICE SYMBOL (If applicable)	7a. NAME OF MONITORING ORGANIZATION Rome Air Development Center (EECT)
6c. ADDRESS (City, State and ZIP Code) Graduate Engineering & Res. School of Engr 300 College Park Dayton OH 45469	7b. ADDRESS (City, State and ZIP Code) Hanscom AFB MA 01731
8a. NAME OF FUNDING/SPONSORING ORGANIZATION Rome Air Development Center 8b. OFFICE SYMBOL (If applicable) EECT	9. PROCUREMENT INSTRUMENT IDENTIFICATION NUMBER F19628-83-K-0034
8c. ADDRESS (City, State and ZIP Code) Hanscom AFB MA 01731	10. SOURCE OF FUNDING NOS

PROGRAM ELEMENT NO.	PROJECT NO.	TASK NO.	WORK UNIT NO
62702F	4600	15	68

11. TITLE (Include Security Classification)
AN ITERATION METHOD FOR COMPLEX SCATTERING PROBLEMS

12. PERSONAL AUTHOR(S)
Michael Kaye, P. Krishna Murthy, Gary A. Thiele

13a. TYPE OF REPORT	13b. TIME COVERED	14. DATE OF REPORT (Yr., Mo., Day)	15. PAGE COUNT
Interim	FROM 051583 TO 051584	October 1984	62

16. SUPPLEMENTARY NOTATION
N/A

17 COSATI CODES			18. SUBJECT TERMS (Continue on reverse if necessary and identify by block number)
FIELD	GROUP	SUB. GR	Scattering,
12	01		Numerical Electromagnetics,
20	14		Diffraction

19. ABSTRACT (Continue on reverse if necessary and identify by block number)

An iteration method for solving an integral representation of Maxwell's equation is presented. In this method, the scattering body is divided into lit and shadow side regions separated by the geometric optics boundary. The total current at any point on the surface of the scatterer, induced by an incident field, is the sum of an approximate optics current and a correction current. Both of these currents are computed by iteration. The general theory is presented and applied to the problem of scattering from a two-dimensional square cylinder. The results are compared with the method of moments and excellent agreement is obtained. Due to its structure, the iteration method, unlike the method of moments, does not give spurious results at internal resonances of the scatterer. The method is applicable to complex structures and can be used for non-perfect conductors.

20. DISTRIBUTION/AVAILABILITY OF ABSTRACT	21. ABSTRACT SECURITY CLASSIFICATION
UNCLASSIFIED/UNLIMITED ☒ SAME AS RPT ☐ DTIC USERS ☐	UNCLASSIFIED

22a. NAME OF RESPONSIBLE INDIVIDUAL	22b. TELEPHONE NUMBER (Include Area Code)	22c. OFFICE SYMBOL
Robert V. McGahan	617-861-2050	RADC (EECT)

DD FORM 1473, 83 APR EDITION OF 1 JAN 73 IS OBSOLETE

UNCLASSIFIED
SECURITY CLASSIFICATION OF THIS PAGE

ABSTRACT

An iteration method for solving an integral representation of Maxwell's equation is presented. In this method, the scattering body is divided into lit and shadow side regions separated by the geometric optics boundary. The total current at any point on the surface of the scatterer, induced by an incident field, is the sum of an approximate optics current and a correction current. Both of these currents are computed by iteration. The general theory is presented and applied to the problem of scattering from a two-dimensional square cylinder. The results are compared with the method of moments and excellent agreement is obtained. Due to its structure, the iteration method, unlike the method of moments, does not give spurious results at internal resonances of the scatterer. The method is applicable to complex structures and can be used for non-perfect conductors.

TABLE OF CONTENTS

LIST OF FIGURES

Figures (continued) Page

I. INTRODUCTION

In this report, a method for computing the electromagnetic scattering properties of complex objects is presented. This method can deal with electrically small or large bodies alike and is not restricted to perfect conductors. It is an iteration method based on an integral representation of Maxwell's equations.

In Chapter 2, a brief review of the integral equations for the electromagnetic field is given. It is shown how they can be combined with impedance boundary conditions in order to deal with non-perfect conductors and as a special case of interest, coated perfect conductors.

Chapter 3 takes a look at the AS-MM hybrid diffraction technique which is the starting point of the iteration method. In this hybrid technique, the current, induced on the surface of a scatterer by an incident field, is approximated by optics currents which are supplemented by correction currents in order to give the true current. The approximate optics currents are computed by iteration, whereas, the correction currents are computed by using the moment method in certain "moment method regions". Although this approach has been shown to be successful for simple geometries, the task of dividing up a complex body into moment method and asymptotic regions is a formidable one. These moment method regions complicate the programming even for perfect conductors let alone non-perfect ones.

In an attempt to do away with the moment method regions, the iteration method was developed. This method is described in Chapter 4. The two methods are basically similar in that they both define the same approximate optics currents and the same correction currents. However, no moment method regions are defined and the correction currents are found by iteration just as are the optics currents.

In Chapter 5, some numerical results for the two-dimensional problem of a square cylinder are exhibited. Results for the iteration method are compared to results obtained by the method of moments, which is considered exact. The results are in general excellent except for small regions in the shadow side for large bodies. This question is examined in Chapter 6 and a possible way of improving the iteration method, by changing the iteration procedure and the approximations made, is suggested. Chapter 7 is devoted to a summary and a few concluding remarks.

2. THE INTEGRAL EQUATIONS FOR SCATTERING FROM NON-PERFECT CONDUCTORS

Consider an arbitrarily shaped non-perfectly conducting body situated in a vacuum. Let the body be illuminated by an incident electromagnetic field $(\vec{E}^i, \vec{H}^i)$. Then the total electric and magnetic fields at an observation point $\vec{R}$ are given by (with suppressed time variation $\exp(j\omega t)$)[1]

$$\vec{E}(\vec{R}) = T\vec{E}^i(\vec{R}) - T \oint_s \{j\beta\eta_o(\hat{n}'x\vec{H}) G(r) - (\hat{n}'x\vec{E})x\vec{\nabla}' G(r) - (\hat{n}' \cdot \vec{E}) \vec{\nabla}' G(r)\} ds' \quad (1)$$

$$\vec{H}(\vec{R}) = T\vec{H}^i(\vec{R}) + T \oint_s \{j \frac{\beta}{\eta_o} (\hat{n}'x\vec{E}) G(r) + (\hat{n}'x\vec{H}) x\vec{\nabla}' G(r) + (\hat{n}' \cdot \vec{H}) \vec{\nabla}' G(r)\} ds' \quad (2)$$

where $T = (1 - \Omega/4\pi)^{-1}$ and $\oint$ is used to denote the principle value integral over s, i.e., the integral over the closed surface excluding an ε neighborhood of the singularity in $G(r)$ at $r = 0$. The absolute value of the solid angle, Ω, subtended by the deformed surface (in taking $\oint$) at the field point $\vec{R}$ must be determined from the geometry of the surface. However, if s is smoooth at $\vec{R}$ then $\Omega = 2\pi$ $(T = 2)$ and if $\vec{R}$ is not located on the surface then $\Omega = 0$ $(T = 1)$. All the parameters and variables (β, η_o, etc.) connected with the electromagnetic field are defined in Appendix A. Note that $\vec{R}$ is allowed to be located on a surface whose tangent is not a differentiable function of position, however, the field is required to possess a finite mean value at $\vec{R}$. Equations (1) and (2) are referred to as the electric field integral equation (EFIE) and the magnetic field integral equation (MFIE).

Introducing the equivalent sources:

$$\vec{J} = \hat{n}x\vec{H}, \qquad \vec{M} = -\hat{n}x\vec{E} \tag{3}$$

Equations (1) and (2) can be rewritten as

$$\vec{E}(\vec{R}) = T\vec{E}^{i}(\vec{R}) - T \oint_{S} \{j\beta n_o \vec{J}\, G(r) + \vec{M}x\vec{\nabla}'\, G(r) - (\hat{n}' \cdot \vec{E})\, \vec{\nabla}'\, G(r)\}\, ds' \tag{4}$$

$$\vec{H}(\vec{R}) = T\vec{H}^{i}(\vec{R}) + T \oint_{S} \{-\frac{j\beta}{n_o} \vec{M}\, G(r) + \vec{J}x\vec{\nabla}'\, G(r) + (\hat{n}' \cdot \vec{H})\, \vec{\nabla}'\, G(r)\}\, ds' \tag{5}$$

where, from Maxwell's equations:

$$\hat{n} \cdot \vec{E} = \frac{jn_o}{\beta} \vec{\nabla}' \cdot \vec{J}, \qquad \hat{n}' \cdot \vec{H} = \frac{j}{\beta n_o} \vec{\nabla}' \cdot \vec{M} \tag{6}$$

The scattered field can be obtained from Equations (4) and (5) as follows:

$$\vec{E}^{s}(\vec{R}) = \vec{E}(\vec{R}) - \vec{E}^{i}(R) \tag{7}$$

$$\vec{H}^{s}(\vec{R}) = \vec{H}(\vec{R}) - \vec{H}^{i}(R) \tag{8}$$

and since for $\vec{R} \notin S$, $T = 1$, Equations (4) and (5) together with (7) and (8) yield

$$\vec{E}^{s}(\vec{R}) = - \int_{S} \{j\beta n_o \vec{J}\, G(r) + \vec{M}x\vec{\nabla}'\, G(r) - (\hat{n}' \cdot \vec{E})\, \vec{\nabla}'\, G(r)\}\, ds' \tag{9}$$

$$\vec{H}^{s}(\vec{R}) = \int_{S} \{-\frac{j\beta}{n_o} \vec{M}\, G(r) + \vec{J}x\nabla'\, G(r) + (\hat{n}' \cdot \vec{H})\, \vec{\nabla}'\, G(r)\}\, ds' \tag{10}$$

The equivalent surface currents can be found from Equations (1) and (2) by considering $\vec{R} \in s$ with s smooth, so that $T = 2$ and a unit vector $\hat{n}$ can be defined at $\vec{R}$ on s. Then upon taking the vector cross product of $\hat{n}$ with (1) and (2) and using Equation (3), Equations (1) and (2) yield:

$$-\vec{M}(\vec{R}) = 2\,\hat{n}\times\vec{E}^{i}(\vec{R}) - 2\,\hat{n}\times\int_{s}\{j\beta\eta_{o}\vec{J}G(r) + \vec{M}\times\vec{\nabla}'G(r) - (\hat{n}'\cdot\vec{E})\,\vec{\nabla}'G(r)\}\,ds' \qquad (11)$$

$$\vec{J}(\vec{R}) = 2\,n\times\vec{H}^{i}(\vec{R}) + 2\,\hat{n}\times\int_{s}\{-\frac{j\beta}{\eta_{o}}\vec{M}G(r) + \vec{J}\times\vec{\nabla}'G(r) + (\hat{n}'\cdot\vec{H})\,\vec{\nabla}'G(r)\}\,ds' \qquad (12)$$

with $\hat{n}'\cdot\vec{E}$ and $\hat{n}'\cdot\vec{H}$ given by Equation (6).

Equations (11) and (12) are two coupled equations for the surface currents $\vec{J}$ and $\vec{M}$, which when computed can be used in Equations (9) and (10) to find the scattered field. These equations can be decoupled by using the impedance boundary conditions [2]:

$$\hat{n}\times\vec{M} = Z\,\vec{J} \qquad (13)$$

or

$$\hat{n}\times\vec{J} = -\frac{1}{Z}\,\vec{M} \qquad (14)$$

On substituting (13) and (14) in (11), (12), and (6), the following decoupled equations are obtained:

$$-\vec{M}(\vec{R}) = 2n\times\vec{E}^{i}(\vec{R}) - 2\hat{n}\times\int_{s}\{\frac{j\beta}{Z_{r}}(\hat{n}\times\vec{M})\,G(r) + \vec{M}\times\vec{\nabla}'\,G(r) - (\hat{n}'\cdot\vec{E})\vec{\nabla}'\,G(r)\}\,ds' \qquad (15)$$

$$\vec{J}(\vec{R}) = 2\hat{n}\times\vec{H}^{i}(\vec{R}) + 2\hat{n}\times\int_{s}\{j\beta Z_{r}(\hat{n}\times\vec{J})\,G(r) + \vec{J}\times\vec{\nabla}'\,G(r) + (\hat{n}'\cdot\vec{H})\,\vec{\nabla}'\,G(r)\}\,ds' \qquad (16)$$

with $\hat{n}'\cdot\vec{E}$ and $\hat{n}'\cdot\vec{H}$ given by:

$$\hat{n}' \cdot \vec{E} = \frac{j}{\beta Z_r} \vec{\nabla}' \cdot (\hat{n}' \times \vec{M}), \quad \hat{n} \cdot \vec{H} = -\frac{jZ_r}{\beta} \vec{\nabla}' \cdot (\hat{n}' \times \vec{J}) \tag{17}$$

Where, $Z_r = Z/n_o$ is the relative surface impedance of the scatterer.

The complexity of the above integral equations can be reduced by considering a specific physical situation. The scatterer that will be considered here is that of a perfect conductor coated with a layer of non-perfectly conducting material. Furthermore, the following assumptions will be made [3]:

1. The index of refraction of the coating is very large and has a large imaginary part. $|N| \gg 1$ and $Im(N) \gg 1$.
2. The fields outside the body vary slowly with respect to the dimension of the interior wavelength.
3. The thickness, d, of the coating, is less than the principal radii of curvature of the outer surface, and $\beta d \ll |N|$
4. The radii of curvature of the surface are large compared to the interior wavelength.

Under these conditions, the wave inside the coating will be TEM with direction of propagation inward and normal to the surface. Hence,

$$\hat{n}' \cdot \vec{E} = \hat{n}' \cdot \vec{H} = 0 \tag{18}$$

and the surface impedance , Z, will be independent of the polarization of the incident radiation and will be given by:

$$Z = j\eta \tan N\beta d \tag{19}$$

which is the expression that would be obtained for Z without the above assumptions but for normal incidence. Finally, it should be noted that when dealing with coated edges, Equation (19) does not hold at the edge or within a few skin depths (of the coating material) from the edge.

Substituting Equations (18) in Equations (15) and (16) yields the following expressions for the surface currents:

$$-\vec{M}(\vec{R}) = 2\hat{n}x\vec{E}^i(\vec{R}) - 2\hat{n}x \oint_s \{\frac{j\beta}{Z_r}(\hat{n}x\vec{M})\ G(r) + \vec{M}x\vec{\nabla}'\ G(r)\}\ ds' \tag{20}$$

$$\vec{J}(\vec{R}) = 2\hat{n}x\vec{H}^i(\vec{R}) + 2\hat{n}x \oint_s j\beta Z_r(\hat{n}x\vec{J})\ G(r) + \vec{J}x\vec{\nabla}'G(r)\}\ ds' \tag{21}$$

whereas, from Equations (9) and (10), the scattered fields are given by

$$\vec{E}^s(\vec{R}) = -\int_s \{j\beta n_o\vec{J}\ G(r) + \vec{M}x\vec{\nabla}'\ G(r)\}\ ds' \tag{22}$$

$$\vec{H}^s(\vec{R}) = \int_s \{ -\frac{j\beta}{n_o}\vec{M}\ G(r) + \vec{J}x\vec{\nabla}'\ G(r)\}\ ds'$$

For a perfect conductor, $\vec{M} = \hat{n}x\vec{E} = \hat{n}\cdot\vec{H} = 0$ and a similar analysis to that given above leads to

$$\hat{n}x\vec{E}^i(\vec{R}) = \hat{n}x \oint_s \{j\beta n_o\ \vec{J}\ G(r) - \frac{jn_o}{\beta}(\vec{\nabla}'\cdot\vec{J})\ \vec{\nabla}'\ G(r)\}\ ds' \tag{23}$$

$$\vec{J}(\vec{R}) = 2\hat{n}x\vec{H}^i(\vec{R}) + 2\hat{n}x \int_s \vec{J}x\vec{\nabla}'\ G(r)\ ds' \tag{24}$$

$$\vec{E}^s(\vec{R}) = -\int_s \{j\beta n_o\ \vec{J}\ G(r) - \frac{jn_o}{\beta}(\vec{\nabla}'\cdot\vec{J})\ \vec{\nabla}'\ G(r)\}\ ds' \tag{25}$$

$$\vec{H}^s(\vec{R}) = \int_s \vec{J}x\vec{\nabla}'\ G(r)\ ds' \tag{26}$$

3. THE AS-MM HYBRID DIFFRACTION TECHNIQUE

The general theory of the AS-MM hybrid diffraction technique is described in detail in [4]. This technique is based on the MFIE as given by Equation (24). The basic approach is to divide the total surface S of the body into S^{ℓ} and S^{s}, which represent the lit and shadowed regions, respectively. The currents in these regions are given by (26), which can now be written as:

$$\vec{J}^{\ell}(R) = 2\hat{n}x\vec{H}^{i}(\vec{R}) + 2\hat{n}x \oint_{S^{\ell}} \vec{J}^{\ell}x\vec{\nabla}' G(r)\, ds' + 2\hat{n}x \oint_{S^{s}} \vec{J}^{s}x\vec{\nabla}' G(r)\, ds' \qquad (27)$$

$$\vec{J}^{s}(\vec{R}) = 2\hat{n}x\vec{H}^{i}(\vec{R}) + 2\hat{n}x \oint_{S^{\ell}} \vec{J}^{\ell}x\vec{\nabla}' G(r)\, ds' + 2\hat{n}x \oint_{S^{s}} \vec{J}^{s}x\vec{\nabla}' G(r)\, ds' \qquad (28)$$

Each region is further divided into an asymptotic (AS) region and a moment method (MM) region. The MM regions are taken to be small regions on either side of the shadow boundary and the AS regions as the remaining regions in S^{ℓ} and S^{s}. In order to be able to solve for $\vec{J}^{\ell}$ and $\vec{J}^{s}$ in the AS and MM regions, it is assumed that $\vec{J}^{s}$ in Equation (27) is small so that it can be neglected. This defines an approximate lit side optics current $\vec{J}^{\ell}_{op}$ given by

$$\vec{J}^{\ell}_{op}(\vec{R}) = 2\hat{n}x\vec{H}^{i}(\vec{R}) + 2\,\hat{n}x \oint_{S^{\ell}} \vec{J}^{\ell}_{op}x\vec{\nabla}' G(r)\, ds' \qquad (29)$$

Then replacing $\vec{J}^{\ell}$ in (28) by $\vec{J}^{\ell}_{op}$ defines an approximate shadow side optics current

$$\vec{J}^{s}_{op}(R) = 2\hat{n}x\vec{H}^{i}(\vec{R}) + 2\hat{n}x \oint_{S^{\ell}} \vec{J}^{\ell}_{op}x\vec{\nabla}' G(r)\, ds' + \hat{2}nx \oint_{S^{s}} \vec{J}^{s}_{op}x\vec{\nabla}' G(r)\, ds' \qquad (30)$$

The exact currents in S^{ℓ} and S^{s} are then given by

$$\vec{J}^{\ell}(\vec{R}) = \vec{J}^{\ell}_{op}(\vec{R}) + \vec{I}^{\ell}(\vec{R}) \tag{31}$$

$$\vec{J}^{s}(\vec{R}) = \vec{J}^{s}_{op}(\vec{R}) + \vec{I}^{s}(\vec{R}) \tag{32}$$

Substituting Equations (31) and (32) into the MFIE (27) and (28) and using (29) and (30), the following expressions for the correction currents $\vec{I}^{\ell}$ and $\vec{I}^{s}$ are found:

$$\vec{I}^{\ell}(\vec{R}) = 2\hat{n}x\int_{S^s} \vec{J}^{s}_{op}x\vec{\nabla}' G(r)\, ds' + 2\hat{n}x\int_{S^{\ell}} \vec{I}^{\ell}x\vec{\nabla}' G(r)\, ds' + 2\hat{n}x\int_{S^s} \vec{I}^{s}x\vec{\nabla}' G(r)\, ds' \tag{33}$$

$$\vec{I}^{s}(\vec{R}) = 2\hat{n}x \int_{S^s} \vec{I}^{s}x\vec{\nabla}' G(r)\, ds' + 2\hat{n}x \int_{S^{\ell}} \vec{I}^{\ell}x\vec{\nabla}' G(r)\, ds' \tag{34}$$

The process that is defined for solving the above system of equations is as follows. $\vec{J}^{\ell}_{op}$ is computed by iterating Equation (29) with $2\hat{n}x\vec{H}^{i}(R)$ the initial current. Then $\vec{J}^{s}_{op}$ is computed by iterating Equation (30) using $2\hat{n}x\vec{H}^{i}(\vec{R}) + 2\hat{n}x\int \vec{J}^{\ell}_{op}x\nabla G(r)\, ds'$ as the initial current. Equations (33) and (34) are now written down for S^{ℓ}_{MM}, S^{ℓ}_{AS}, S^{s}_{MM} and S^{s}_{AS}. The correction currents in the MM regions are now computed by neglecting the integrals over the correction currents in the AS regions. It is argued that without ignoring those current terms containing integrals over I^{ℓ}_{AS} and I^{s}_{AS} in the expressions for $\vec{I}^{\ell}_{MM}(\vec{R})$ and $\vec{I}^{s}_{MM}(\vec{R})$, it is not possible to derive sets of equations which can be solved by the moment method. The correction currents in the AS regions can now be computed by integrating over the moment method correction currents, again ignoring those current terms containing integrals over $\vec{I}^{\ell}_{AS}$ and $\vec{I}^{s}_{AS}$.

The above process defines a first-order approximation. A second-order approximation is obtained by substituting the values obtained for $\vec{I}^{\ell}$ and $\vec{I}^{s}$ in the MM and AS regions in the integrals for $\vec{I}^{\ell}_{MM}(\vec{R})$, $\vec{I}^{s}_{MM}(\vec{R})$, $\vec{I}^{\ell}_{AS}(\vec{R})$ and $\vec{I}^{s}_{AS}(\vec{R})$

but this time without neglecting the integrals over $\dagger I^{\ell}_{AS}$ and $\dagger I^{s}_{AS}$. Higher order approximations are obtained in a similar fashion.

It was found in [4] that it was necessary to use second-order, and in some cases, third-order approximations to yield a good value for the current. However, no criterion was found for fixing the size of the MM regions.

4. THE ITERATION METHOD

The iteration method is based on the AS-MM hybrid technique and is an attempt to do away with the MM regions of the latter. Hence, the exact current is written as

$$\vec{J}(\vec{R}) = \vec{J}_{op}(\vec{R}) + \vec{I}(\vec{R}) \tag{35}$$

and the surface of the scatterer is divided into lit and shadow regions separated by the geometrical optics shadow boundary. $\vec{J}^{\ell}_{op}(\vec{R})$ and $\vec{J}^{s}_{op}(\vec{R})$ are given by Equations (29) and (30), respectively, and are solved by iteration. The initial currents for S^{ℓ} and S^{s} being the same as those of the AS-MM hybrid method.

Having solved for the optics currents, the correction currents are now considered. Instead of using MM regions as in AS-MM, Equations (33) and (34) are now solved by iteration just as the optics current were. Only one approximation is called for here and that is the neglecting of the integral over $\vec{I}^{s}$ in Equation (33). In second- and higher-order approximations, this integral is put back in Equation (33).

The full set of equations for the iteration method will be given below. These equations are based on Equations (20) and (21) describing the magnetic and electric surface currents induced on a perfect conductor coated with a thin layer of material with a very large refractive index. The magnetic correction currents will be denoted by $\vec{N}$. Hence, the exact magnetic current is given by

$$\vec{M}(\vec{R}) = \vec{M}_{op}(\vec{R}) + \vec{N}(\vec{R}) \tag{36}$$

Since the equations are rather cumbersome for the general case, the following two operators will be defined:

$$L[\vec{J}] = 2\hat{n}x \int_S \vec{J}x\vec{\nabla}' \, G(r) \, ds' \tag{37}$$

$$K[\vec{J}] = 2\hat{n}x \int_S j\beta(\hat{n}xJ) \, G(r) \, ds' \tag{38}$$

The optics currents are given by:

$$\vec{J}^{\ell}_{op} = 2\hat{n}x\vec{H}^{i} + K[\vec{J}^{\ell}_{op}Z_r] + L[\vec{J}^{\ell}_{op}] \tag{39}$$

$$\vec{J}^{s}_{op} = 2\hat{n}x\vec{H}^{i} + K[\vec{J}^{\ell}_{op}Z_r] + L[\vec{J}^{\ell}_{op}] + K[\vec{J}^{s}_{op}Z_r] + L[\vec{J}^{s}_{op}] \tag{40}$$

$$\vec{M}^{\ell}_{op} = -2\hat{n}xE^{i} + K[\vec{M}^{\ell}_{op}/Z_r] + L[\vec{M}^{\ell}_{op}] \tag{41}$$

$$\vec{M}^{s}_{op} = -2\hat{n}xE^{i} + K[\vec{M}^{\ell}_{op}/Z_r] + L[\vec{M}^{\ell}_{op}] + K[\vec{M}^{s}_{op}/Z_r] + L[\vec{M}^{s}_{op}] \tag{42}$$

The correction currents are given by:

$$\vec{I}^{\ell} = K[\vec{I}^{\ell}Z_r] + L[\vec{I}^{\ell}] + K[\vec{J}^{s}_{op}Z_r] + L[\vec{J}^{s}_{op}] + \{K[\vec{I}^{s}Z_r] + L[\vec{I}^{s}]\} \tag{43}$$

$$\vec{I}^{s} = K[\vec{I}^{\ell}Z_r] + L[\vec{I}^{\ell}] + K[\vec{I}^{s}Z_r] + L[\vec{I}^{s}] \tag{44}$$

$$\vec{N}^{\ell} = K[\vec{N}^{\ell}/Z_r] + L[\vec{N}^{\ell}] + K[\vec{M}^{s}_{op}/Z_r] + L[\vec{M}^{s}_{op}] + \{K[\vec{N}^{s}/Z_r] + L[\vec{N}^{s}]\} \tag{45}$$

$$\vec{N}^{s} = K[\vec{N}^{\ell}/Z_r] + L[\vec{N}^{\ell}] + K[\vec{N}^{s}/Z_r] + L[\vec{N}^{s}] \tag{46}$$

The case of a perfect conductor can be retrieved from these equations by setting $\hat{M} = \hat{N} = 0$ and then $Z_r = 0$. The terms in the braces are set to zero for the first-order calculation.

5. THE SQUARE CYLINDER

The first application of the iteration method to be considered is that of a two-dimensional cylinder of a square cross section. The computer program for the iteration method was set up to solve for the electric currents only, since, as can be seen from Equations (39) - (46), the magnetic currents can be obtained from the same program by simply performing the duality transformation:

$$\vec{J} \longrightarrow \vec{M}$$

$$\vec{I} \longrightarrow \vec{N}$$

$$\vec{H} \longrightarrow -\vec{E}$$

$$Z_r \longrightarrow 1/Z_r \tag{47}$$

The geometry under consideration is shown in Figure 1. The computer program uses the angle of incidence θ^i, although the complementary angle α will also be referred to here. For a two-dimensional scattering problem

$$G(r) = \frac{1}{4j} H_o^{(2)}(\beta r) \tag{48}$$

$$\vec{\nabla}' G(r) = -\frac{\beta}{4j} H_1^{(2)}(\beta r) \tag{49}$$

where $H_o^{(2)}$ and $H_1^{(2)}$ are the Hankel functions of the second kind of order zero and one, respectively. Due to symmetry, the angle of incidence can be restricted to

$$45^0 \leq \alpha < 90^0 \tag{50}$$

where the case of grazing incidence has been omitted for the time being. With the above restriction, sides 1 and 4 are the lit sides, whereas sides 2 and 3 are the shadow sides. The distance d along the perimeter of the cylinder is measured in an anticlockwise direction from the origin of the coordinate system which is situated at the corner A.

The incident field is given by

$$\vec{q}^{\,i} = \hat{Z}\, e^{-j\beta \hat{u} \cdot \vec{R}} \tag{51}$$

where, $\hat{u}$ is the direction of propagation of the incident field and $\vec{R}$ is the radius vector to the observation point.

For the case of a perfectly conducting square cylinder, as for any structure comprised of planar surfaces, the principle value integrals reduce to ordinary integrals due to the fact that the $L[\vec{J}]$, or $L[\vec{I}]$, terms are identically zero for the integration and the observation point on the same side of the cylinder. However, the introduction of a finite conductivity gives rise to $K[\vec{M}]$, and $K[\vec{N}]$ terms for which the principle value does have to be taken. The calculation of these terms is discussed in Appendix B.

Figures 2 and 3 show the magnitude and phase, respectively, of the electric current on a .705λ wide cylinder with a surface impedance of Z_r = (.56, - .16). The computation was carried out for the first order only. Due to the poor result as compared to the method of moments, MM, computation (considered exact) [5], the same run was made again, but this time for a perfect conductor. The results are shown in Figures 4 and 5. Despite the fact that the overall agreement is much better this time, there is still an unexplained discrepancy at the lit edge A.

In an attempt to solve this specific problem and at the same time to retain the problem at a reasonable level of complexity, the case of interest was restricted to that of a perfect conductor.

Clearly, there is some difficulty involved in computing the currents close to the edge of the cylinder. In order to understand this problem, consider what happens when computing the optics current at $\vec{R}$ on side 1:

$$\vec{J}'_{op}(\ell_1) = 2\hat{n}xH^i + 2\hat{n}x \int_{\ell'_4} \vec{J}^4_{op}(\ell'_4)\, x\vec{\nabla}' G(r)\, d\ell'_4 \tag{52}$$

where $\vec{R} = \ell_1\hat{x}$ and $\vec{R}' = \ell'_4\hat{y}$. Then, for field points close to the edge A ($\ell_1 \to 0$) and integration points close to A ($\ell'_4 \to 0$), the distance $r = |\vec{R} - \vec{R}'| \to 0$ and the Hankel function has the following small parameter behavior:

$$H_1^{(2)}(\beta r) \approx j\,\frac{2}{\pi\beta r} \tag{53}$$

Numerical integration of the inverse distance function $1/r$ as $r \to \infty$ calls for very samll subdivisions in order to minimize the error. The closer the edge is approached, the smaller the subintervals would have to be. This process is clearly unfavorable since the computation time would increase correspondingly. An analytical evaluation of Equation (52) (for details see Appendix C) as $\ell_1 \to 0$ and $\ell'_4 \to 0$ yields

$$J'_{op}(\ell_1 \to 0) = 2H^i(\ell_1 \to 0) - \frac{1}{2} J^4_{op}(\ell'_4 \to 0) \tag{54}$$

Numerically integrating the integral in (52) for points close to the edge, but avoiding numerical instability, would mean that the minimum possible

values of ℓ, and ℓ_4' would be about 0.02λ and hence the edges would be truncated. In Figure 4, the minimum value of approach to the edges, δ, was taken to be $\delta = .01\lambda$ giving an all around instability. On the other hand, Equation (54) sets no lower bound on the value of δ, so that the edges can be left intact.

The result of numerically integrating Equation (52) with the minimum values of ℓ_1 and ℓ_4' given by $\delta = 0.02\lambda$ is shown in Figures 6 and 7 which show, respectively, the magnitude and the phase of the current induced on a 0.6λ side square cylinder for $\alpha = 45^0$. Notice the overall discrepancy between the current computed by MM and that computed by the iteration method. Figures 8 and 9 show the vast improvement obtained by using Equation (54) for the iteration method, with the minimum values of ℓ_1 and ℓ_4' taken to be $\delta = 10^{-6}\lambda$. This value was henceforth taken as the fixed minimum value for δ. The influence of the order of the approximation can be seen by comparing Figures 10 and 11, a first order calculation, with Figures 8 and 9, a third order calculation. As can be seen, there is an overall improvement in the value of the magnitude of the current in going from first order to third order, except in the deep shadow region.

Further third order results for $\delta = 10^{-6}\lambda$ are shown in Figures 12 to 21. Figures 12 to 15 are for $\alpha = 45^0$, $w = 2.4\lambda$ and $w = 3.7\lambda$, whereas Figures 16 to 21 are for $\alpha = 65^0$, $w = .6\lambda$, 2.4λ and 3.7λ.

6. IMPROVING THE ITERATION METHOD

The final result of any iteration method is dependent on the initial value used to start off the iteration procedure. As already explained in Chapters 2 and 3, the present iteration method is based on the AS-MM so that $\vec{J}^{\ell}_{op}$ is iterated first with an initial value of $2\hat{n}x\vec{H}^{i}$ and then $\vec{J}^{s}_{op}$ is iterated with an initial value of $2\hat{n}x\vec{H}^{i} + 2\hat{n}x \int \vec{J}^{\ell}_{op} x\vec{\nabla} G(r)\, ds'$. Figures 22 and 23 show the resulting magnitude of the optics current as compared with the MM for $W = .6\lambda$ and 3.7λ and $\alpha = 65^{0}$. Note that in both cases, the shadow side optics current is much closer to the true current than the lit side optics current.

The process described above involves taking the shadow side current as zero when iterating the lit side current. This explains the relatively smooth slow varying result obtained for the lit side optics current, for there are no iterations with the shadow side at this stage. On the other hand, when computing the shadow side current, interaction with the lit side is taken into account. This explains why the shadow side optics current follows more closely the true current than does the lit side optics current.

A possible solution to this problem would be to start off by computing $\vec{J}^{s}_{op}$ and taking $\vec{J}^{\ell}_{op}$ as $2\hat{n}xH^{i}$. This would allow for interaction between the shadow side and a reasonable approximation for the lit side. Having iterated $\vec{J}^{s}_{op}$, the lit side optics current can be computed using $\vec{J}^{s}_{op}$ which would give a much better result than formerly when $\vec{J}^{s}_{op}$ was taken as zero. This approach, as well as others, will be tried out in the near future.

7. CONCLUSION

An iteration method for solving the MFIE and the EFIE for a general scatterer has been presented. This method is similar to the AS-MM hybrid technique in that the true surface current is written as the sum of approximate optics currents and correction currents on the lit and shadow side regions of the body. The two methods differ in the way in which the correction currents are computed. In the hybrid technique the lit and shadow areas are further subdivided into moment method and asymptotic regions, the former being the smaller. The MM region correction currents are then solved by using the method of moments, while neglecting their interaction with the asymptotic regions. The asymptotic correction currents are then obtained by integrating the moment method region currents numerically, while again neglecting the interaction between the asymptotic region. These interactions are accounted for in second-order and higher approximations. In the iteration method, the correction currents are obtained by iteration just as the optics currents are. The only approximation made when computing the correction currents via the iteration method being the neglecting of the contribution of the shadow side correction current when computing the lit side correction current. Again, in second- and higher-order approximations this contribution is taken into account.

As an example, the case of a two-dimensional cylinder of square cross section was considered. The currents obtained by the iteration method were compared to the currents obtained by the method of moments. The overall excellent agreement, except for small regions in the shadow region for large bodies, suggests that the order of the iteration process should be changed, viz., the shadow side optics currents should be computed first and then the lit side optics currents. This small discrepancy in the shadow region does

not, however, minimize the importance of the iteration method which has successfully done away with the necessity of a moment method region on the surface of the scatterer.

The formalism was shown to be adaptable to problems of non-perfect conductors, and the special case of a coated perfect conductor was considered.

Finally, it is pointed out that the iteration method does not give erroneous results for geometries having an interior resonance due to the fact that the inhomogeneous integral equation for the surface current is formulated as two inhomogeneous integral equations, one for the optics currents and one for the correction currents and neither of these currents alone can sustain a zero tangential field at the surface of the scatterer. The iteration method has another advantage over the moment method in that it can be used for electrically large bodies that the MM cannot handle, since it is not limited by computer storage.

REFERENCES

1. Poggio, A. J. and E. K. Miller, "Integral Equation Solutions of Three-Dimensional Scattering Problems," in Computer Techniques for Electromagnetics, R. Mittra, Ed. Pergamon Press, New York, 1973, Ch. 4.

2. T.B.A. Senior, "Impedance Boundary Conditions for Imperfectly Conducting Surfaces," Appl. Sci. Res., Vol. 8(B), 1960, pp. 418-436.

3. Crispin, J. W., Jr., and K. M. Siegel, "Method of Radar Cross Section Analysis," Academic Press, New York, 1968.

4. Kim, T. J. and G. A. Thiele, "A Hybrid Diffraction Technique, General Theory and Application," IEEE Trans. Ant. Prop., Vol. AP-30, No. 5, Sept. 1982, pp. 888-897.

5. Richmond, J. H., "An Integral-Equation Solution for TE Radiation and Scattering from Conducting Cylinders," Report 2902-7, The Ohio State Univerity ElectroScience Laboratory; Department of Electrical Engineering, April 1973.

6. Harrington, R. F., "Time-Harmonic Electromagnetic Fields," McGraw-Hill, New York, 1961.

7. Erdélyi, A., "Asymptotic Expansions," Dover Publications, New York, 1956.

8. Abramowicz, M. and I. A. Stegun, "Handbook of Mathematical Functions," National Bureau of Standards, Washington, 1970.

APPENDIX A

DEFINITION OF ELECTROMAGNETIC QUANTITIES

The complex dielectric constant is given by

$$\varepsilon = \varepsilon' - j\varepsilon'' = \varepsilon_o(\varepsilon_r' - j\varepsilon_r'') = \varepsilon_o\varepsilon_r = \varepsilon_o\varepsilon_r'(1 - j\tan\delta_\varepsilon)$$

The complex magnetic permeability is given by

$$\mu = \mu' - j\mu'' = \mu_o(\mu_r' - j\mu_r'') = \mu_o\mu_r = \mu_o\mu_r'(1 - j\tan\delta_\mu)$$

A prime denotes the real part of a complex quantity

A double prime denotes the imaginary part of a complex quantity

A small subscript o refers to vacuum

A small subscript r means that quantity relative to the same quantity in vacuum.

$\varepsilon_r' = \frac{\varepsilon'}{\varepsilon_o}$ = dielectric constant

$\varepsilon_r'' = \frac{\sigma}{\varepsilon_o\omega}$, where σ = conductivity

$\mu_r' = \frac{\mu'}{\mu_o}$ = relative permeability

$\mu_r'' = \frac{\mu''}{\mu_o}$ = relative magnetic loss factor

δ_μ is the magnetic loss angle

δ_ε is the dielectric loss angle

$N = \sqrt{\varepsilon_r \mu_r}$ = complex refractive index

$\beta = \omega \sqrt{\varepsilon \mu}$ = complex propagation constant

$\beta = \beta' - j\beta''$

hence, $\beta = \beta_o N, \qquad \lambda = \lambda_o / N$

$\eta = \sqrt{\frac{\mu}{\varepsilon}} = \eta_r \eta_o$ = absolute impedance of medium

$\eta_r = \sqrt{\frac{\mu_r}{\varepsilon_r}}$ = relative impedance of medium

$\eta_o = \sqrt{\frac{\mu_o}{\varepsilon_o}}$ = free space impedance

$\omega\mu = \beta\eta$

$\omega\varepsilon = \frac{\beta}{\eta}$

$\delta = \frac{1}{\beta''}$ = skin depth

where

$$\beta'' = \frac{\beta_o}{\sqrt{2}} \left[(\mu_r''\varepsilon_r'' - \mu_r'\varepsilon_r') + \sqrt{(\mu_r'\varepsilon_r' - \mu_r''\varepsilon_r'')^2 + (\varepsilon_r'\mu_r'' + \varepsilon_r''\mu_r')} \right]^{1/2}$$

APENDIX B

CALCULATION OF THE PRINCIPLE VALUE INTEGRALS

The integrals defined by Equation (38) are singular as $r \to o$. These integrals are computed by dividing them into subintervals which are integrated separately. The subinterval containing the singularity is of the form

$$I = \int_{-\delta/2}^{\delta/2} H_o^{(2)}(\beta\ell)\, d\ell \tag{B.1}$$

and is computed by taking its principle value. Here, ℓ is a length parameter and δ is the size of the subinterval.

The accuracy of the above integration depends on the width, δ, and on the approximation used for the asymptotic expansion of the Hankel function. The usual small argument expression used for $H_o^{(2)}$ is [6]:

$$H_o^{(2)}(\beta\ell) \approx 1 - j\frac{2}{\pi} \ell n(\frac{1}{2} \gamma\beta\ell) \tag{B.2}$$

substituting (B.2) in (B.1) yields a principle value of

$$I \approx \delta\{1 - j\frac{2}{\pi} \ell n(\frac{\gamma\beta\delta}{4e})\} \tag{B.3}$$

where $\ell n\gamma = .57721566$ is Euler's constant and e is the natural base of logarithms.

The values of $H_o^{(2)}$ as given by (B.2) can be compared with its exact values and it is found that Eq. (B.2) is in error for $(\ell/\lambda) > .02$, giving rise to an error in Eq. (B.3). From asymptotic analysis [7], we know that we can use larger values of (ℓ/λ) and decrease the error by including higher order

terms. The asymptotic expansion for $H_o^{(2)}$ including terms of the order $(\beta\ell)^2$ is [8]

$$H_o^{(2)}(\beta) \approx [1 - \tfrac{1}{4}(\beta\ell)^2]\,[1 - j\tfrac{2}{\pi}\,\ell n(\tfrac{1}{2}\,\gamma\beta\ell)] - \tfrac{j}{2\pi}(\beta\ell)^2 \qquad (B.4)$$

yielding the following expression for the principle value of the integral I:

$$I \approx \delta\{[1 - \tfrac{1}{48}(\beta\delta)^2]\,[1 - j\tfrac{2}{\pi}\,\ell n(\tfrac{\gamma\beta\delta}{4e})] - \tfrac{j}{72\pi}(\beta\delta)^2\} \qquad (B.5)$$

Equation (B.4) is accurate for values of $(\ell/\lambda) < .1$. For a value of $\delta = .12\lambda$, Eq. (B.3) has an error of 1.4% in comparison to Eq. (5), which can be considered exact for this value of δ.

APPENDIX C

CALCULATION OF THE EDGE CURRENTS

In this appendix, the result given in Eq. (63) will be derived. The derivation will be given for a wedge of internal angle α. The geometry involved and the definitions of the various quantities are described in Figure 24. The equation to be considered is

$$\vec{J}^A(\ell) = 2\hat{n}x\vec{H}^i(\ell) + 2\hat{n}x \int \vec{J}^B(\ell')x\vec{\nabla}' G(r)\, d\ell' \qquad (C.1)$$

Now consider the integral

$$\vec{I}(\ell) = 2\hat{n}x \int \vec{J}^B(\ell')\, x\vec{\nabla}' G(r)\, d\ell' \qquad (C.2)$$

where

$$\vec{J}^B(\ell') = J^B(\ell')\hat{t}', \qquad \vec{\nabla}' G = \frac{j\beta}{4} H_1^{(2)}(\beta r)\, \hat{r}'$$

therefore

$$\vec{I}(\ell) = \frac{j\beta}{2} \int \hat{n}x(\hat{t}'x\hat{r}')J^B(\ell')H_1^{(2)}(\beta r)\, d\ell' \qquad (C.3)$$

Now

$$\hat{n}x(\hat{t}'x\hat{r}') = \hat{n}x[\hat{t}'x\{(\hat{r}' \cdot \hat{t}')\hat{t}' + (\hat{r}' \cdot \hat{n}')\hat{n}'\}]$$

$$= \hat{t}(\hat{r}' \cdot \hat{n}') = \hat{t}\cos\psi$$

hence,

$$\bar{I}(\ell) = \frac{j\beta}{2}\,\hat{t}\int_{\ell'=0}^{L} J^{B}(\ell')\,H_1^{(2)}\cos\psi\,d\ell' \tag{C.4}$$

where $\cos\psi = \frac{\ell}{r}\sin\alpha$ (C.5)

and $r = \sqrt{\ell'^2 + \ell^2 - 2\ell\,\ell'\cos\alpha}$ (C.6)

Using the small argument expansion for $H_1^{(2)}$:

$$H_1^{(2)}(\beta r) \approx j\,\frac{2}{\pi\beta r}$$

we get,

$$\bar{I}(\ell) = \frac{j\beta}{2}\,\hat{t}\int_{0}^{L} J^{B}(\ell')\left[j\,\frac{2}{\pi\beta r}\right]\left[\frac{\ell_o \sin\alpha}{r}\right]d\ell'$$

where L is much greater than ℓ and βr is much smaller than unity. The above expansion for the Hankel function can be used since we are only interested in a small neighborhood around the edge. Therefore,

$$\bar{I}(\ell) = -\,\hat{t}\,J^{B}(\ell' + o)\,\frac{\ell\sin\alpha}{\pi}\int_{o}^{L}\frac{d\ell'}{\ell'^2 + \ell^2 - 2\ell'\ell\cos\alpha} \tag{C.7}$$

This is a standard integral which can be integrated to give

$$\bar{I}(\ell) = -\,\frac{\hat{t}}{\pi}\,J^{B}(\ell' + o)\left[\tan^{-1}\left(\frac{L-\ell\cos\alpha}{\ell\sin\alpha}\right) - \tan^{-1}(-\cot\alpha)\right]$$

therefore,

$$\vec{I}(\ell \to o) = -\frac{\hat{t}}{\pi} J^B(\ell' \to o) \left[\tan^{-1}\infty - \tan^{-1}(-\cot\alpha)\right]$$

$$= -\frac{\hat{t}}{\pi} J^B(\ell' \to o) \left[\frac{\pi}{2} - \alpha + \frac{\pi}{2}\right]$$

$$= -\hat{t}\, J^B(\ell' \to o) \left[\frac{\pi - \alpha}{\pi}\right] \qquad (C.8)$$

Substituting Eq. (C.8) in (C.1) with $\ell \to o$ gives:

$$\vec{J}^A(\ell \to o) = 2\hat{n}x\vec{H}^i(\ell \to o) - \hat{t}\, J^B(\ell' \to o)\, (\frac{\pi - \alpha}{\pi})$$

or

$$J^A(\ell \to o) = 2H^i(\ell \to o) - J^B(\ell' \to o)\, (\frac{\pi - \alpha}{\pi}) \qquad (C.9)$$

For the example considered in this report

$\alpha = \pi/2$, hence $\frac{\pi - \alpha}{\pi} = \frac{1}{2}$.

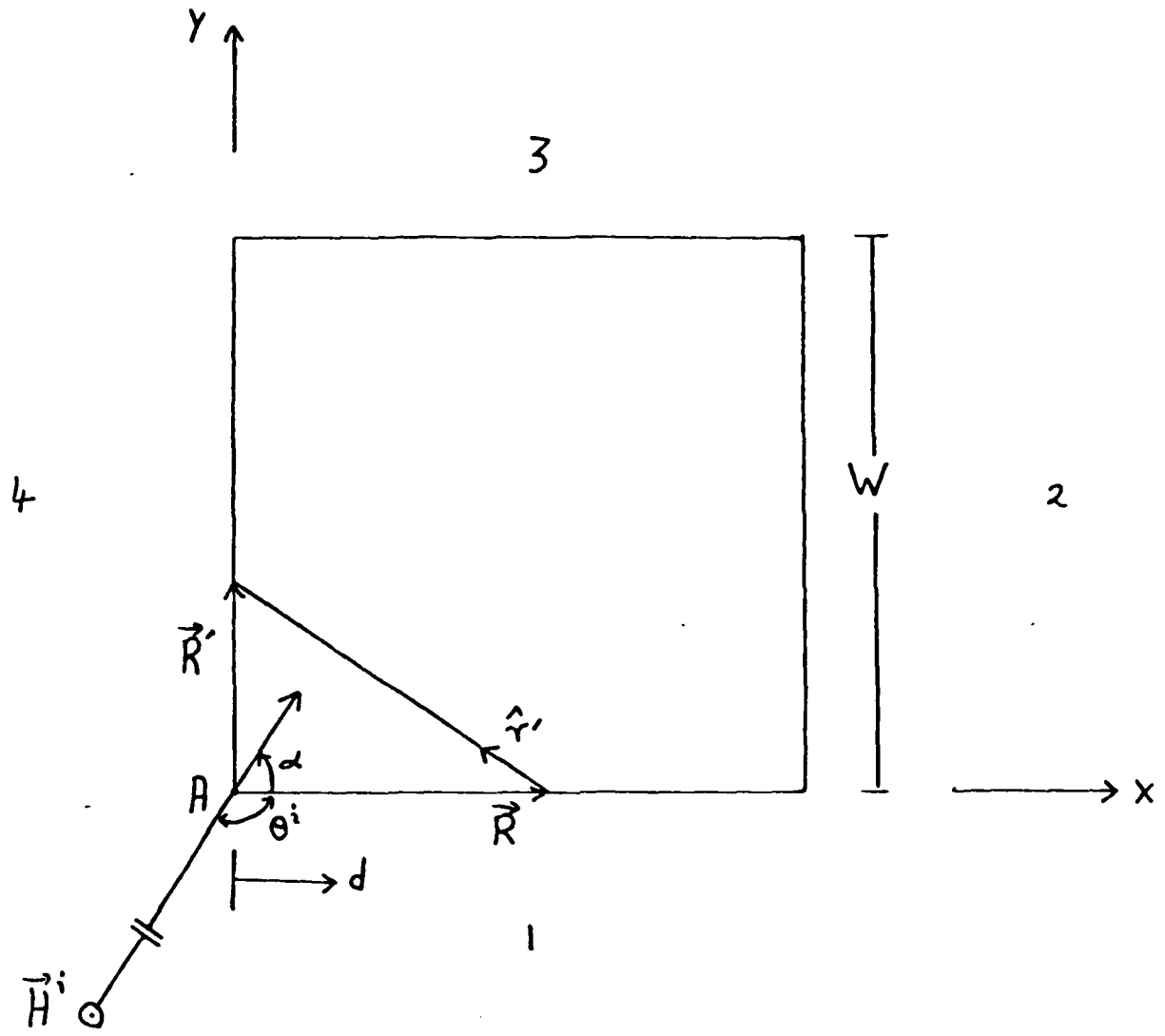

Figure 1. Geometry considered.

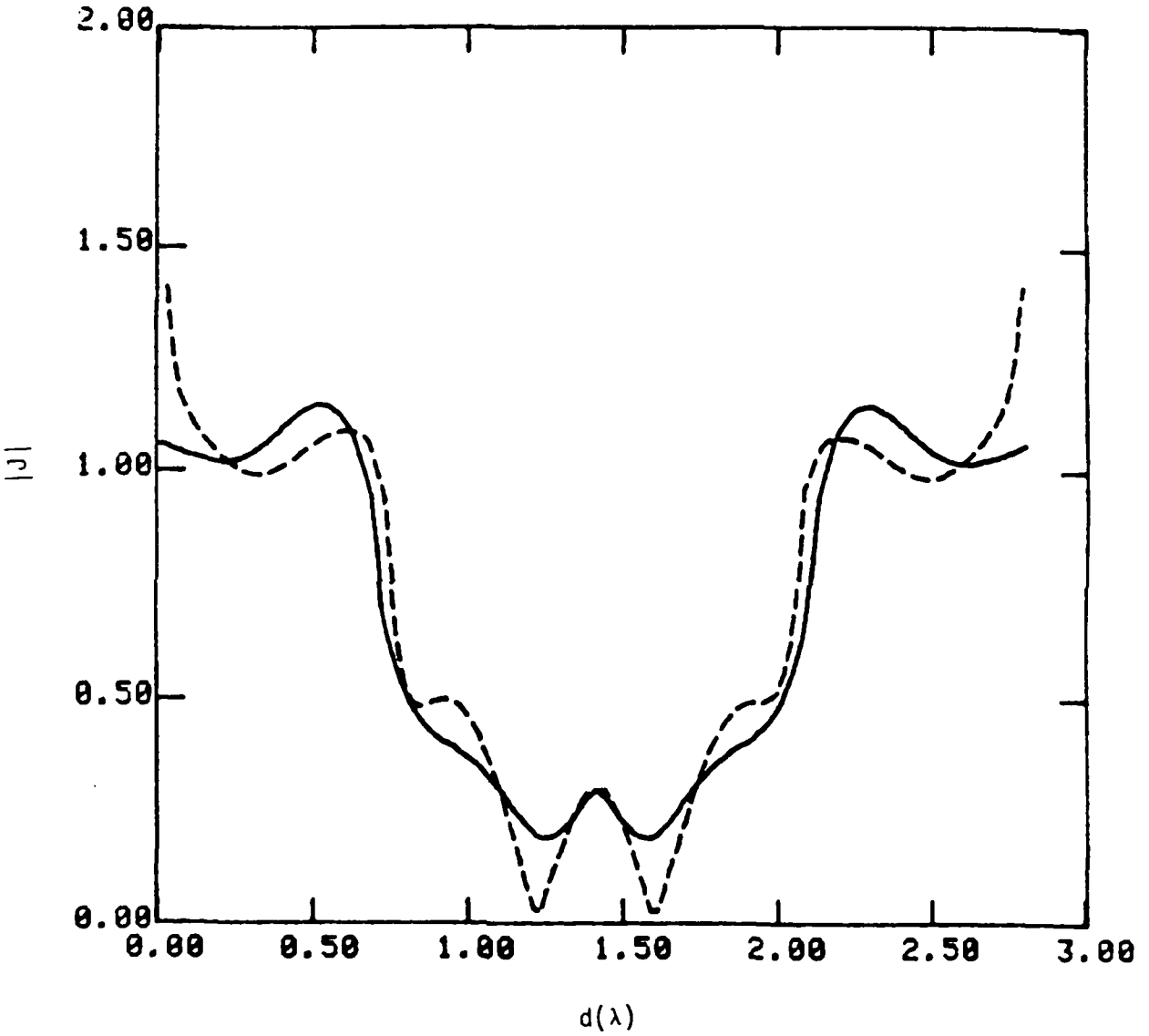

Figure 2. Magnitude of current on cylinder
$W = 0.705\lambda$, $\alpha = 45^0$ and $Z_r = (.56, -.16)$
_____ MM
- - - - - - - - - - Iteration Method

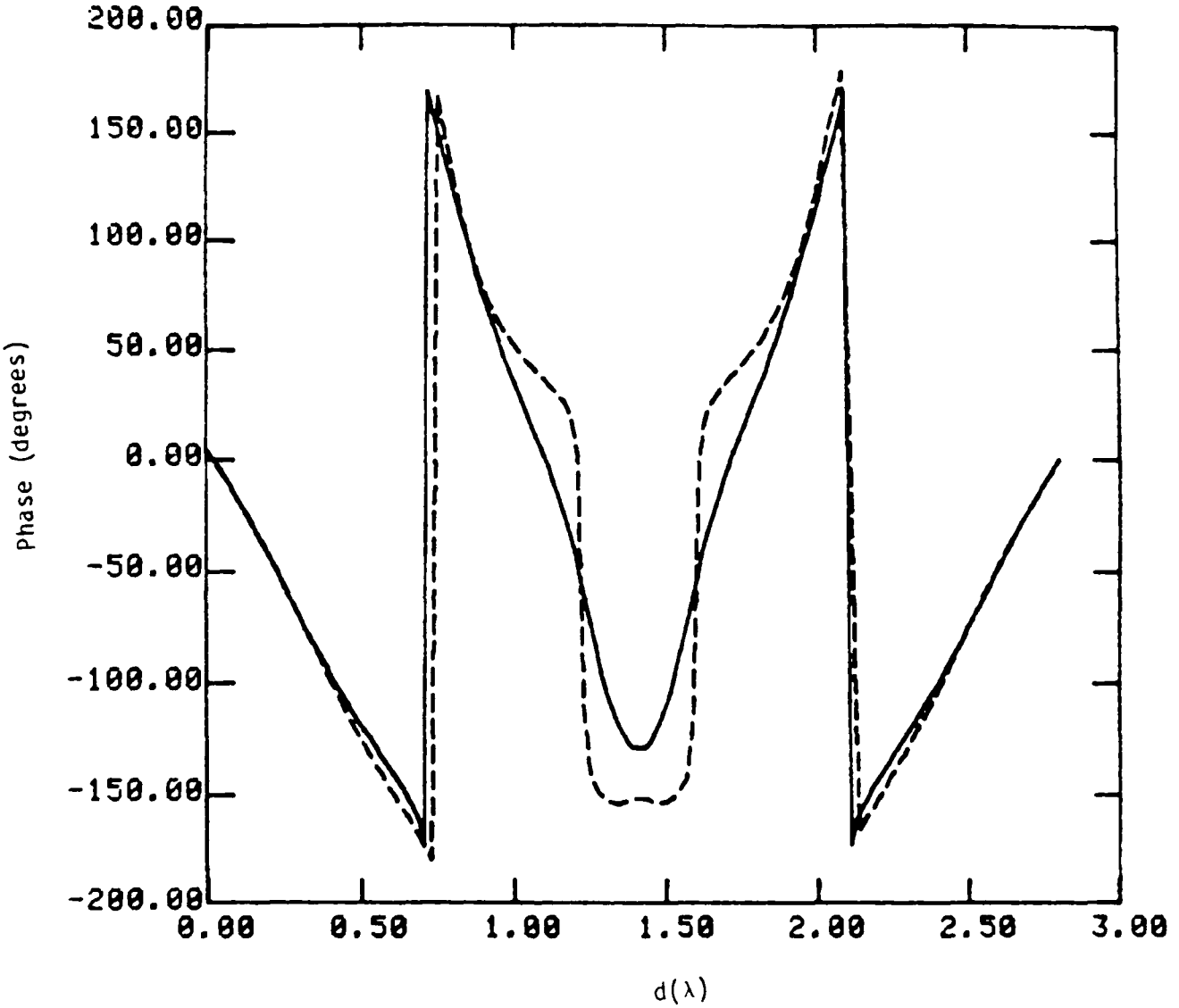

Figure 3. Phase of current on cylinder
$W = 0.705\lambda$, $\alpha = 45^0$ and $Z_r = (.56, -.16)$
_____ MM
- - - - - - - - - - Iteration Method

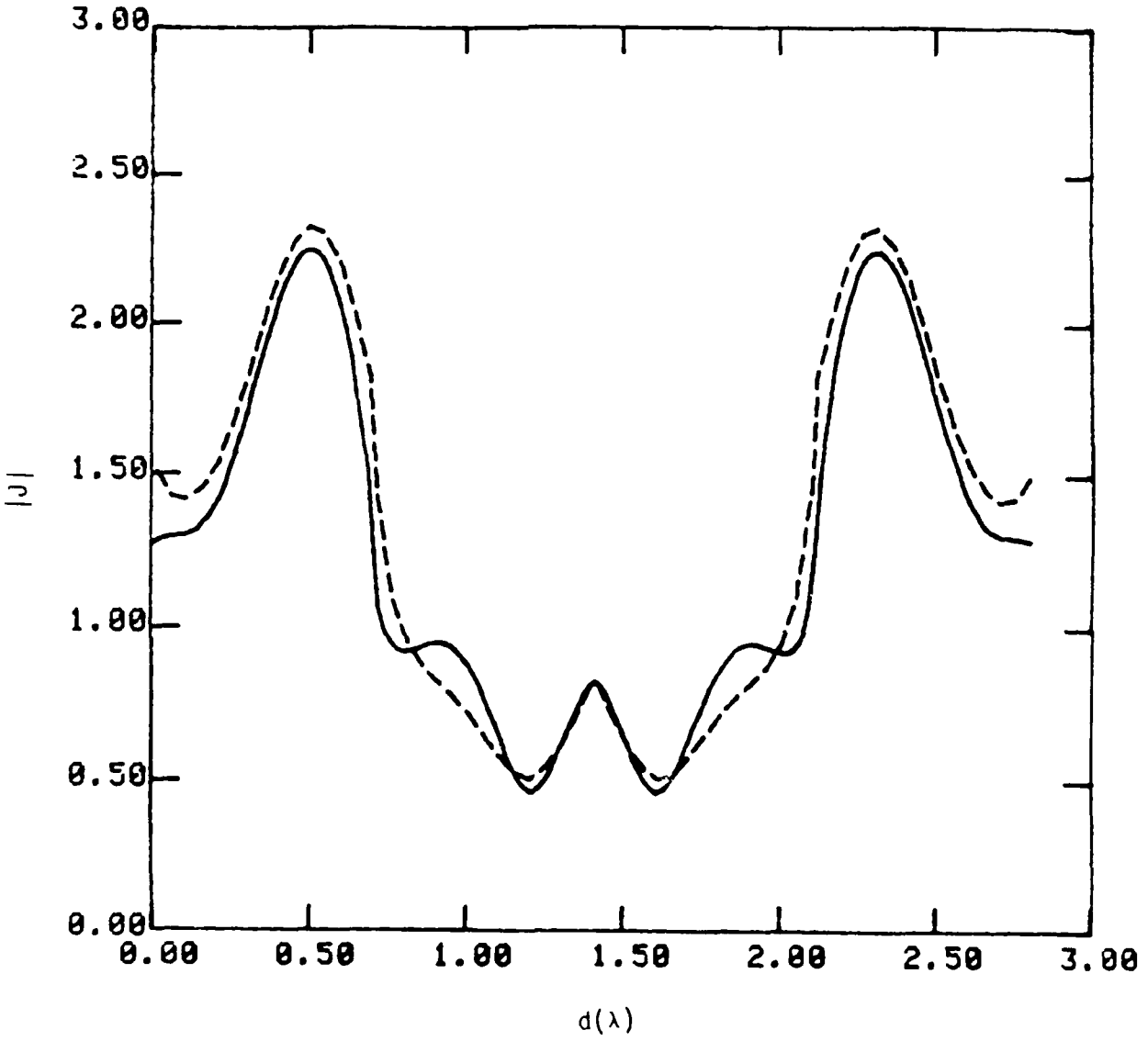

Figure 4. Magnitude of current on cylinder
$W = 0.705\lambda$, $\alpha = 45^0$
_____ MM
- - - - - - - - - - Iteration Method

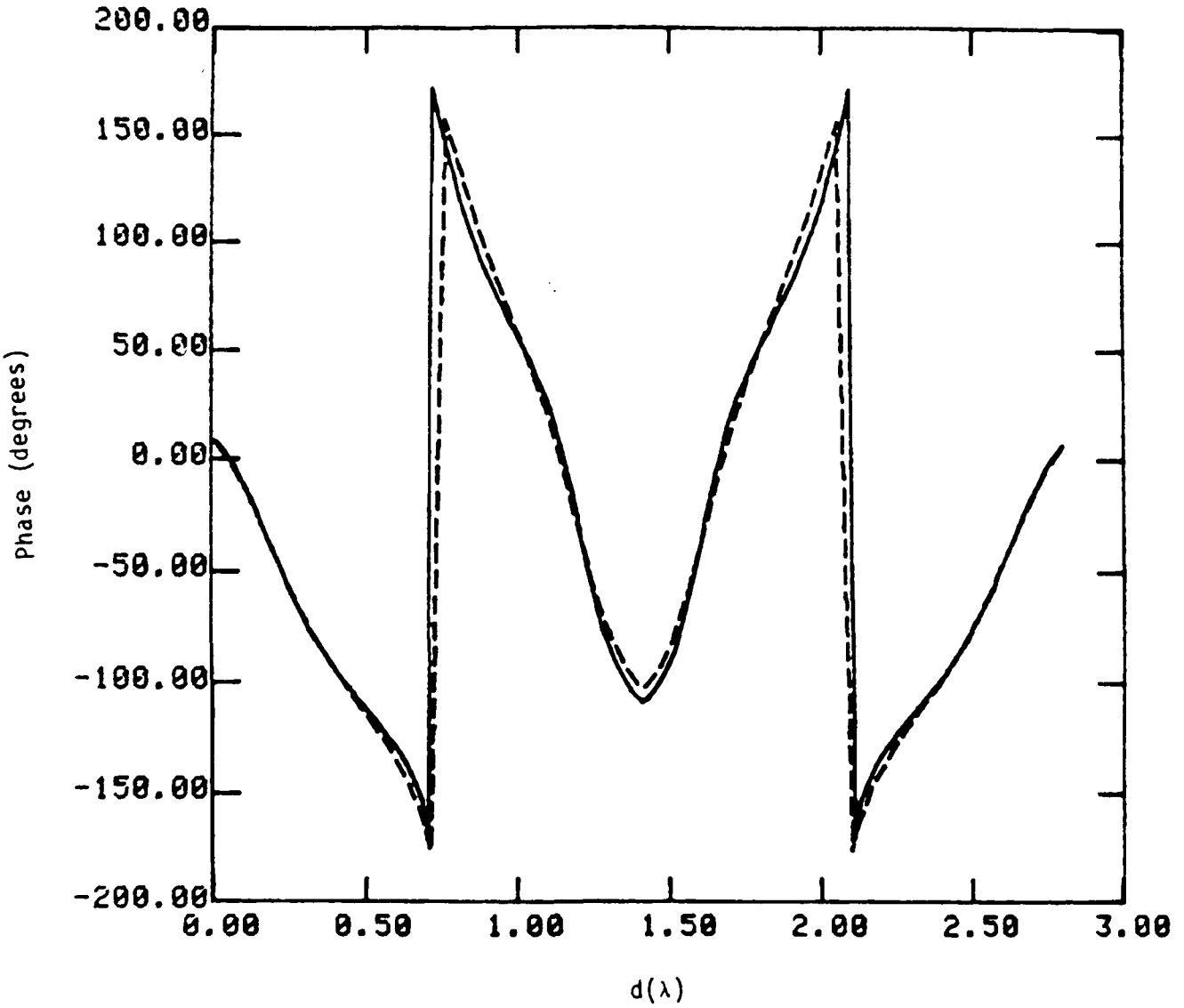

Figure 5. Phase of current on cylinder
$W = 0.705\lambda$, $\alpha = 45^0$
———— MM
- - - - - - - - - Iteration Method

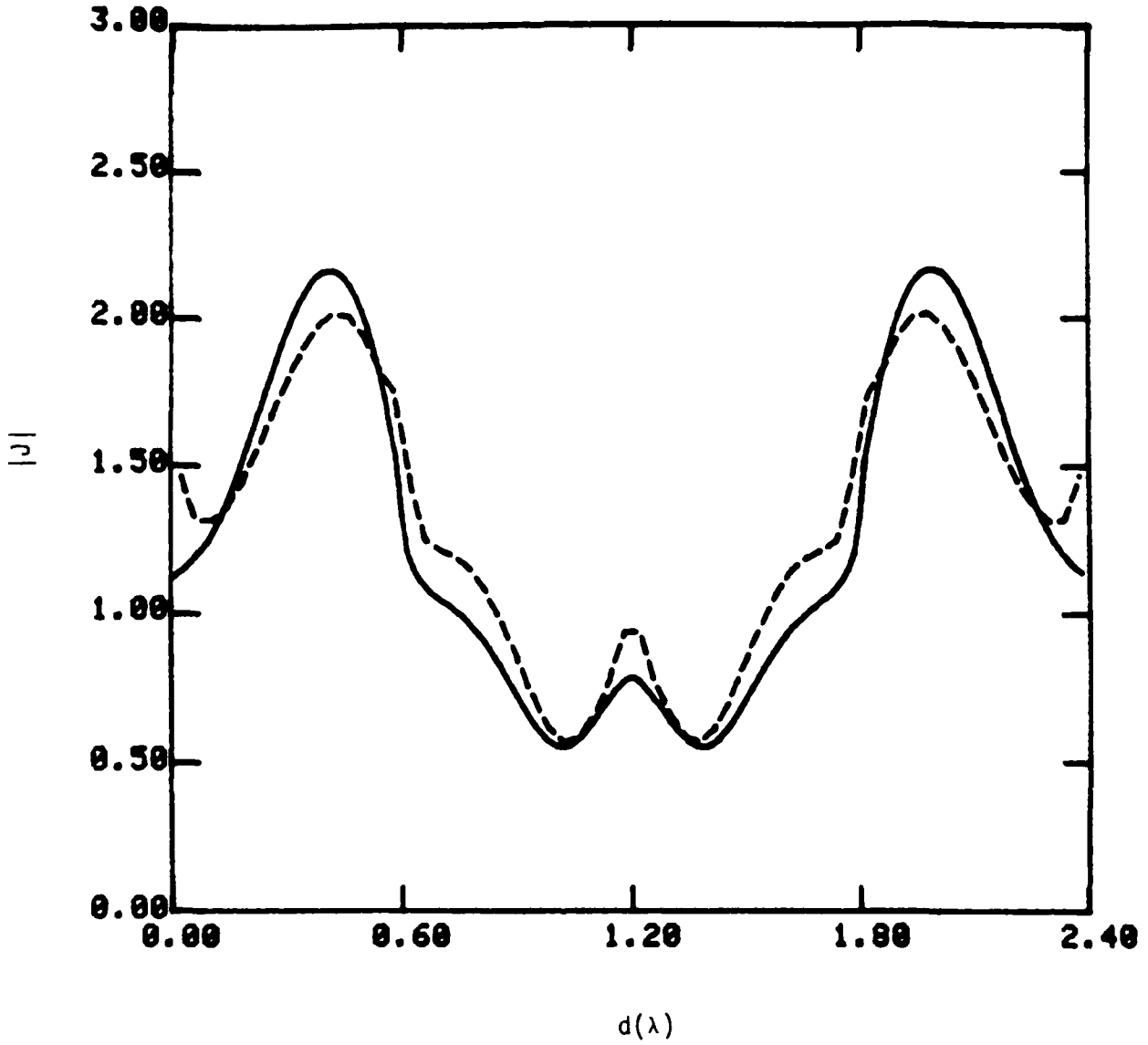

Figure 6. Magnitude of current on cylinder with edge truncation, $\delta = 0.02\lambda$ $W = 0.6\lambda$, $\alpha = 45^0$

———— MM

- - - - - - - - - - Iteration Method

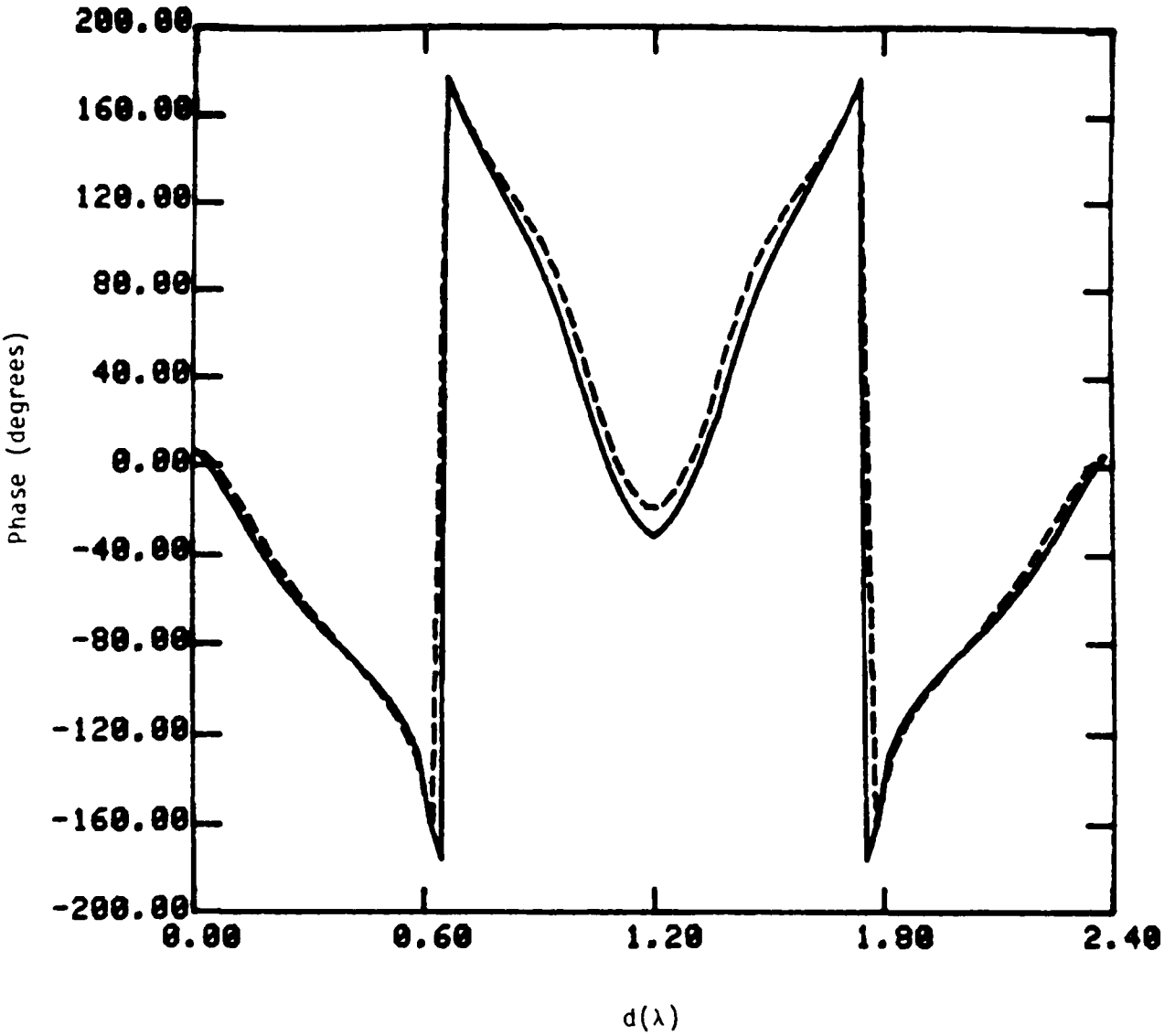

Figure 7. Phase of current on cylinder with edge truncation, $\delta = 0.02\lambda$ $W = 0.6\lambda$, $\alpha = 45^0$

———— MM

- - - - - - - - - - Iteration Method

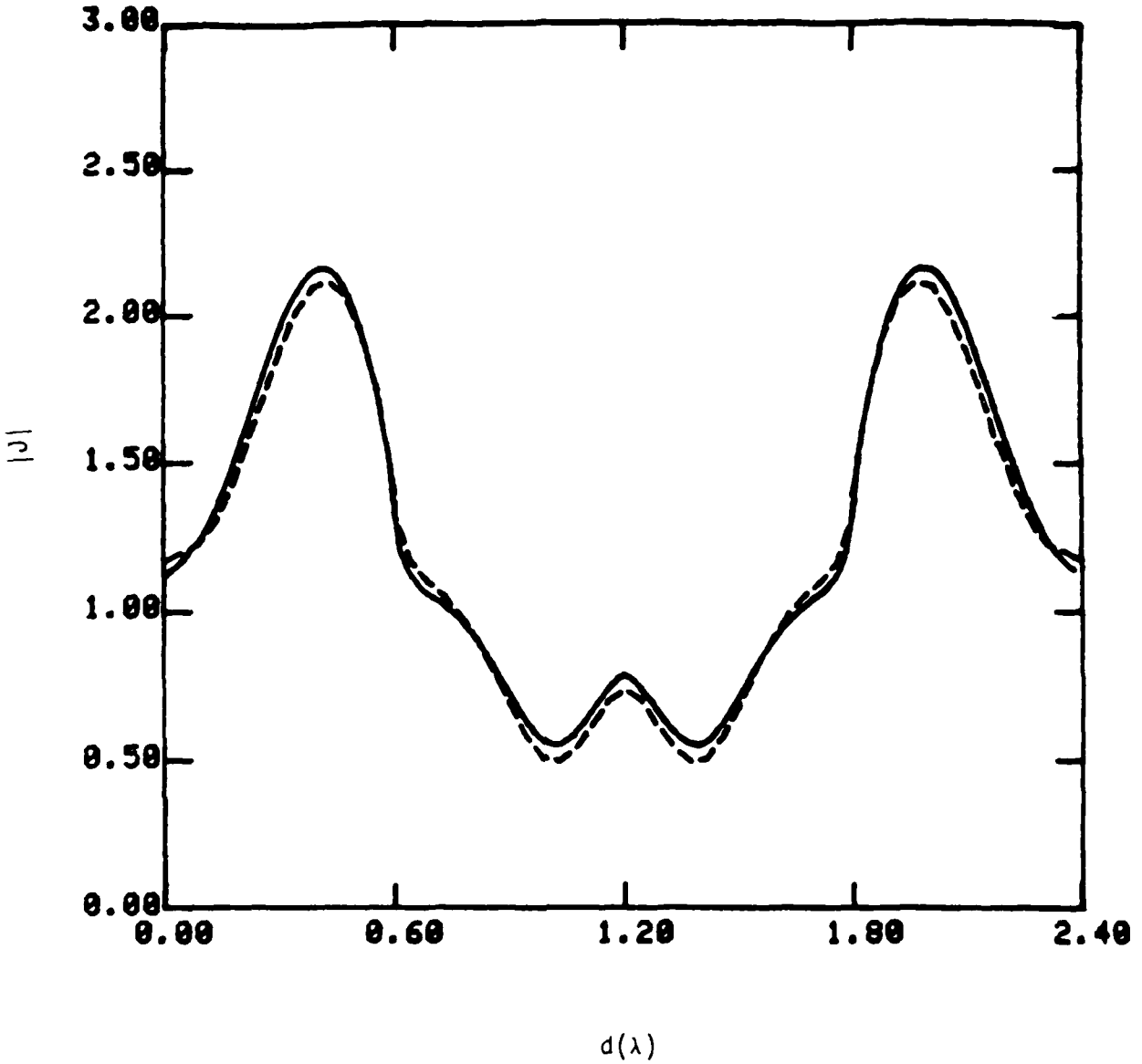

Figure 8. Magnitude of current on cylinder
$W = 0.6\lambda$, $\alpha = 45°$
_____ MM
- - - - - - - - - Iteration Method (3rd order)

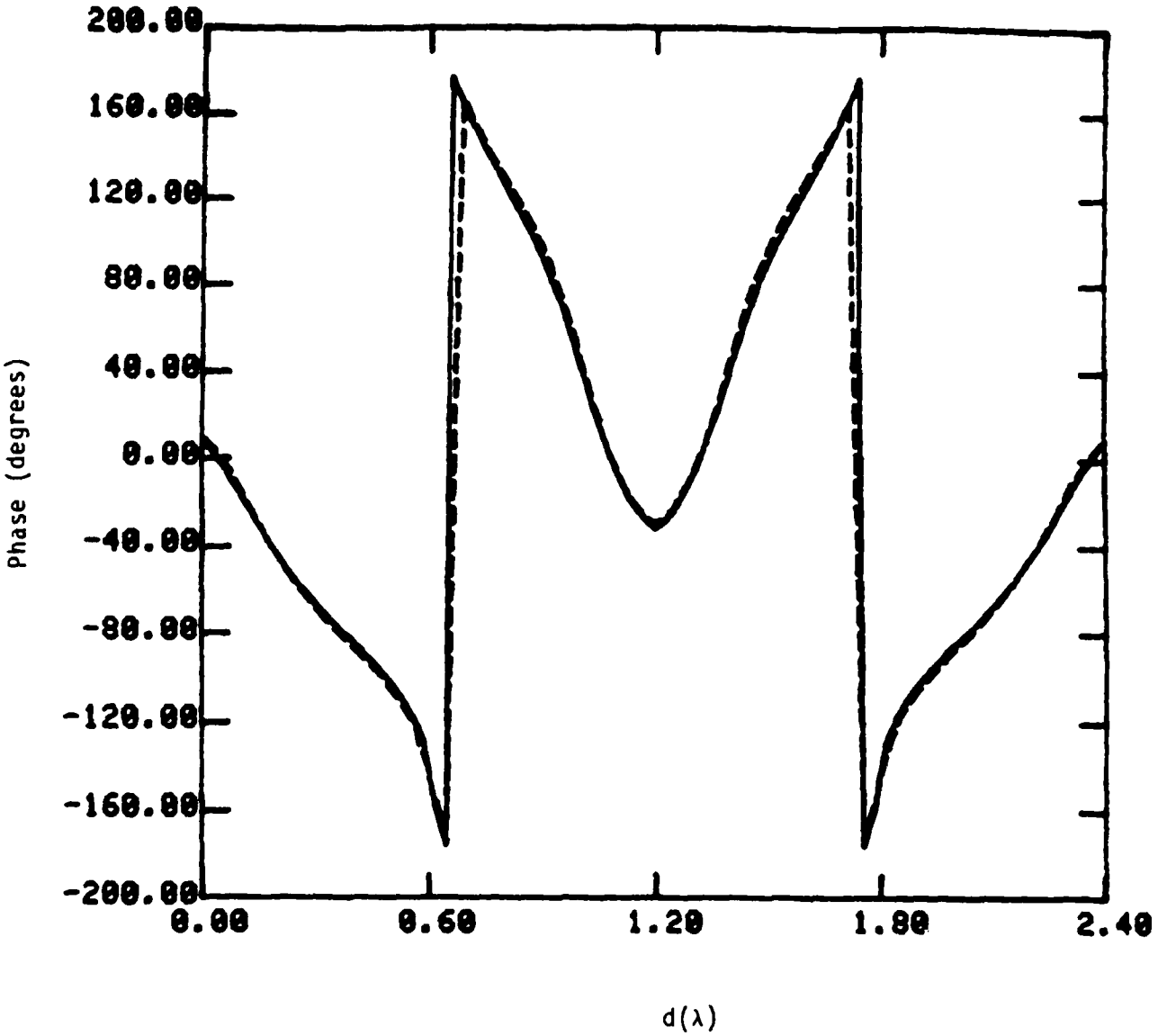

Figure 9. Phase of current on cylinder
$W = 0.6\lambda$, $\alpha = 45^0$
MM
_____
- - - - - - - - - Iteration (3rd order)

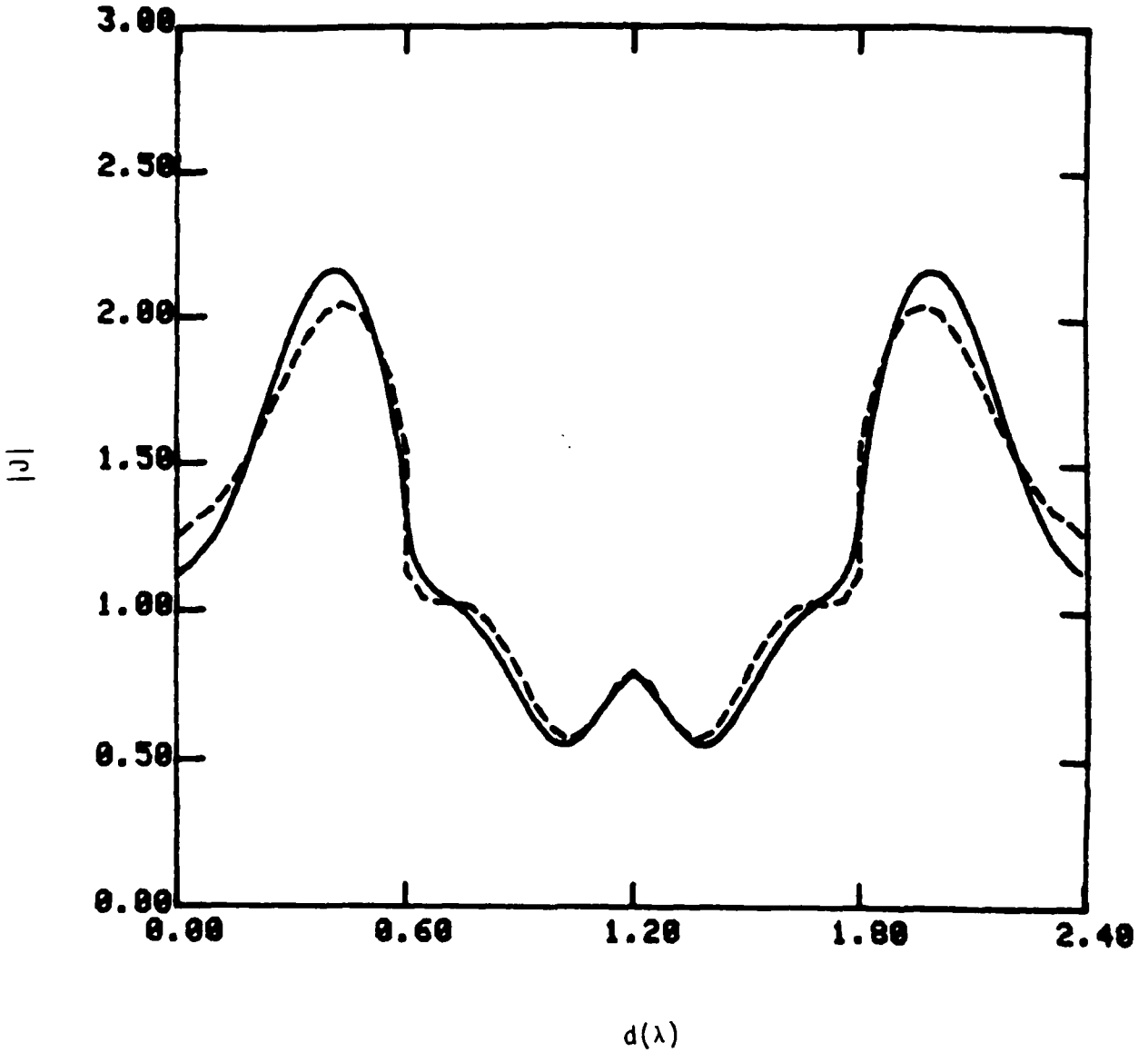

Figure 10. Magnitude of current on cylinder
$W = 0.6\lambda$, $\alpha = 45^0$
———— MM
- - - - - - - - - - Iteration Method (1st order)

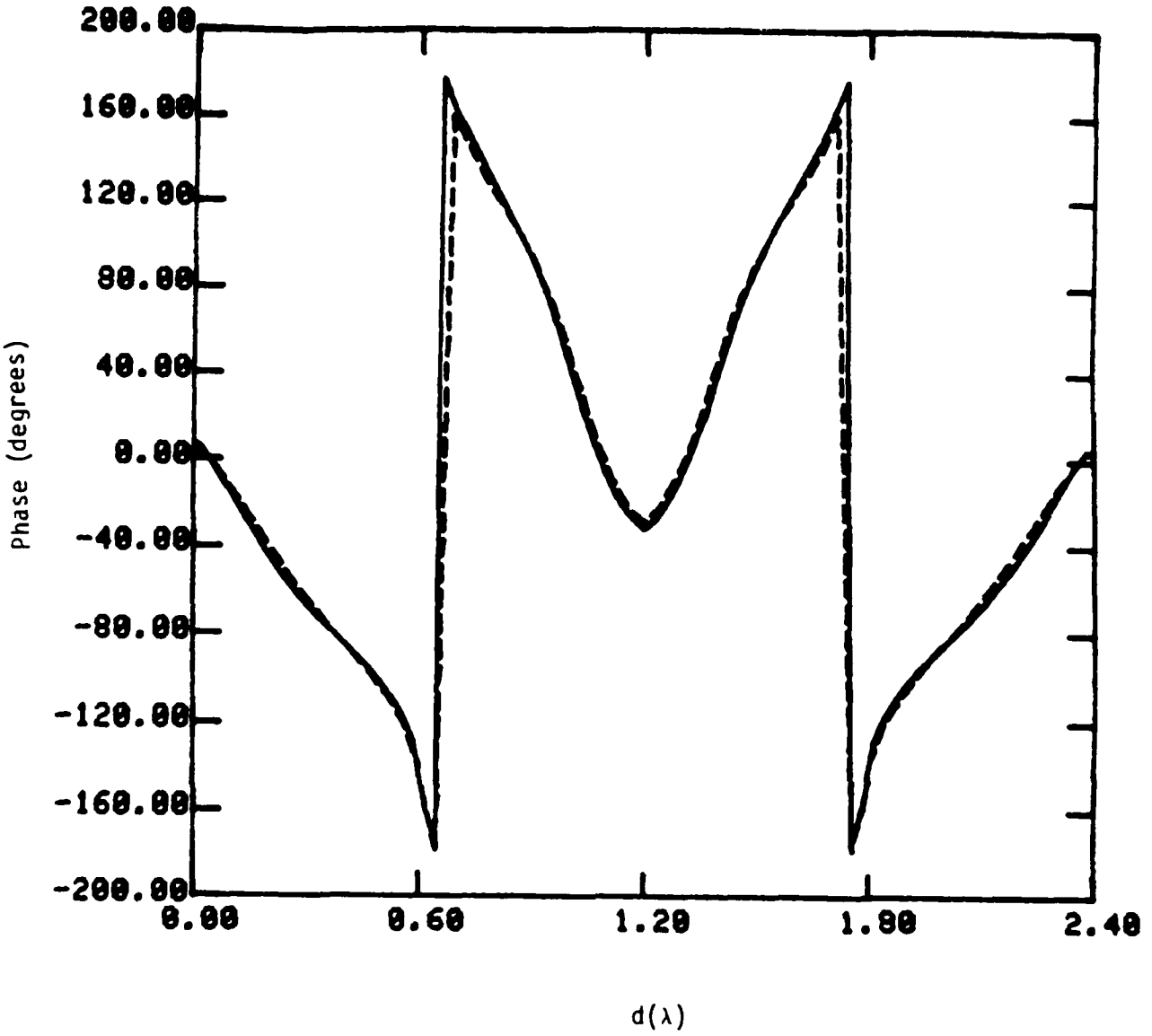

Figure 11. Phase of current on cylinder
$W = 0.6\lambda$, $\alpha = 45^0$
_____ MM
- - - - - - - - - - Iteration Method (1st order)

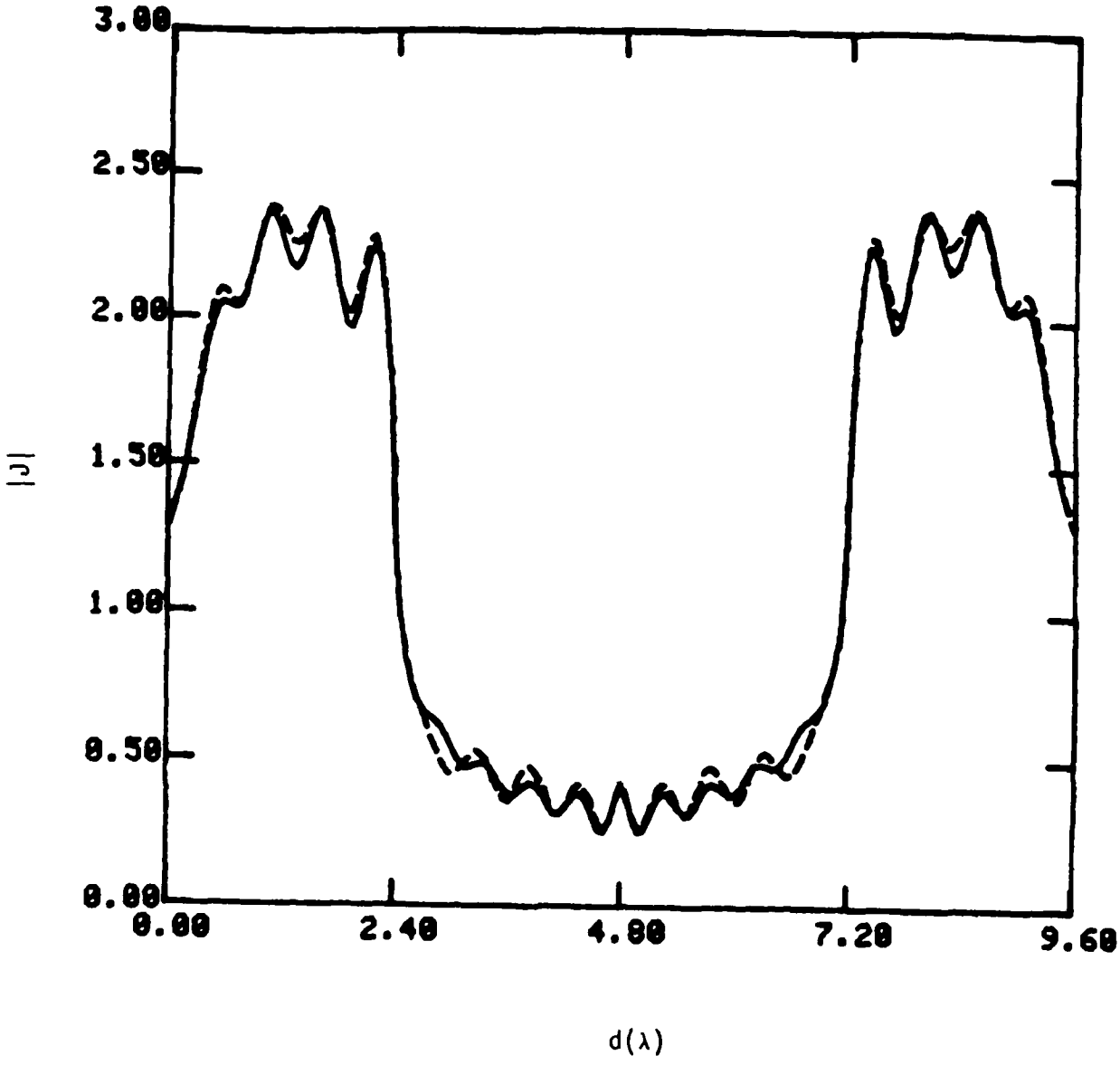

Figure 12. Magnitude of current on cylinder
$W = 2.4\lambda$, $\alpha = 45^0$
——————— MM
- - - - - - - - - Iteration Method

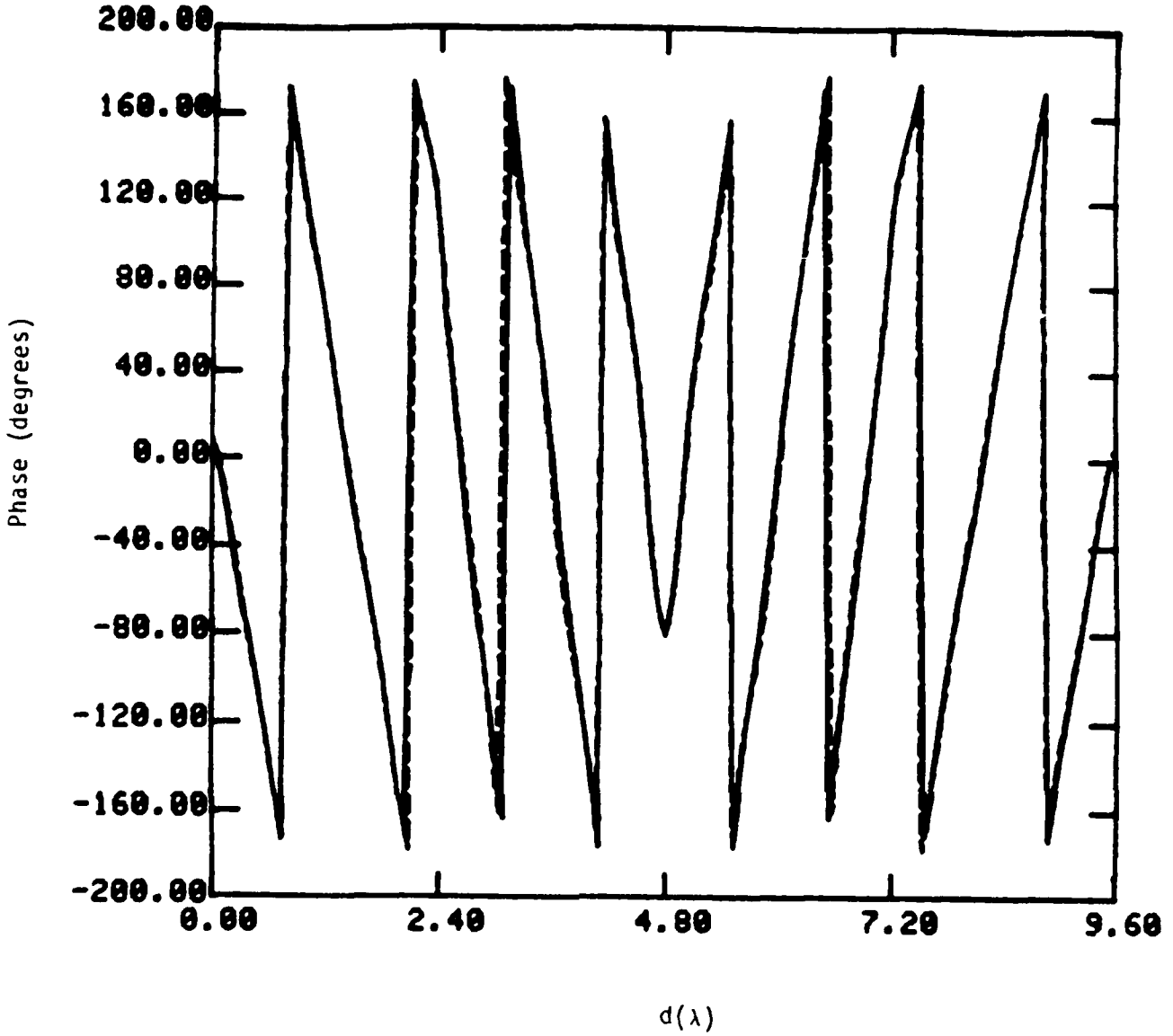

Figure 13. Phase of current on cylinder
$W = 2.4\lambda$, $\alpha = 45^0$
_____ MM
- - - - - - - - - - Iteration Method

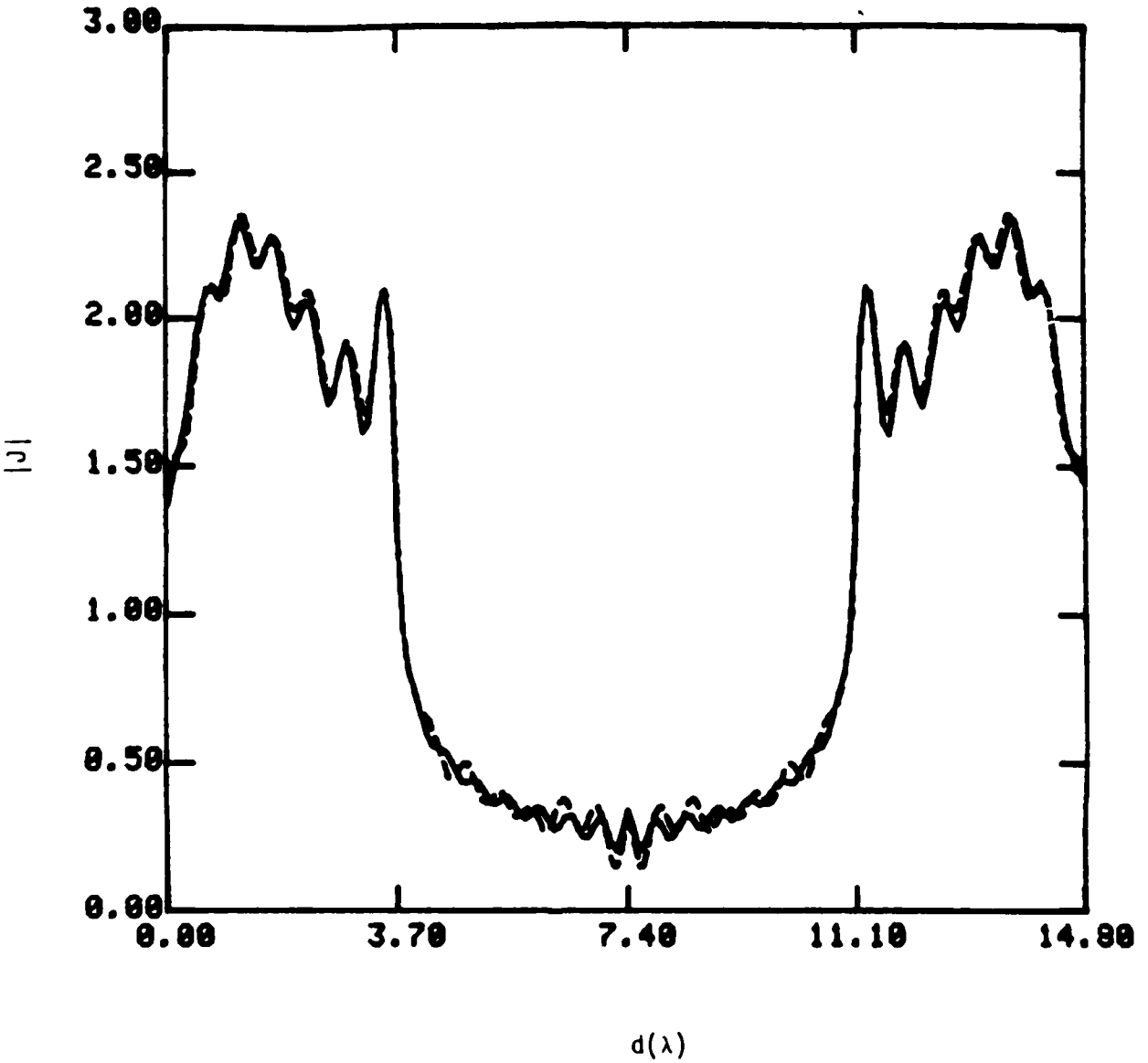

Figure 14. Magnitude of current on cylinder
$W = 3.7\lambda$, $\alpha = 45^0$
——————— MM
- - - - - - - - - - Iteration Method

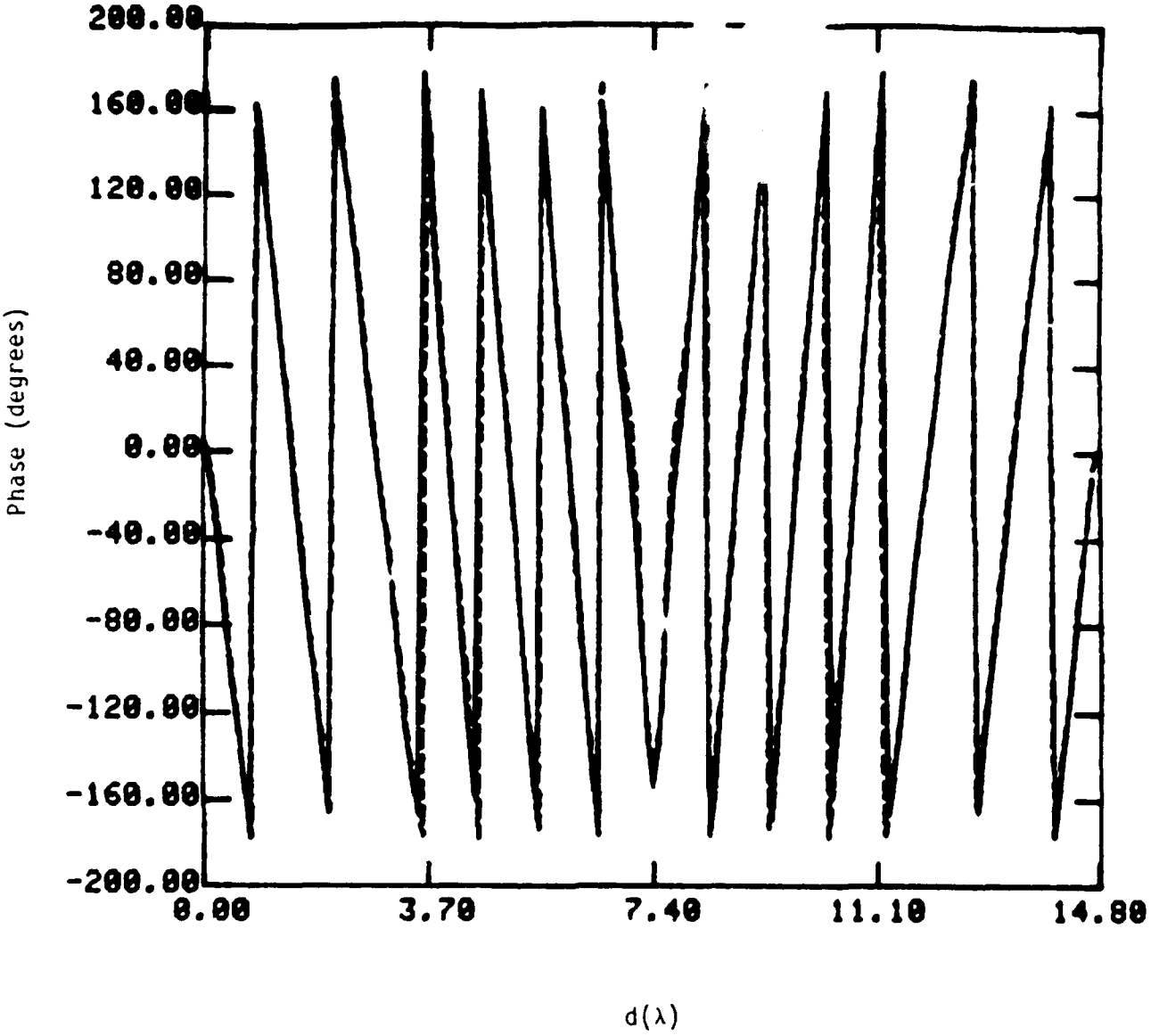

Figure 15. Phase of current on cylinder
$W = 3.7\lambda$, $\alpha = 45^0$
_____ MM
- - - - - - - - - - Iteration Method

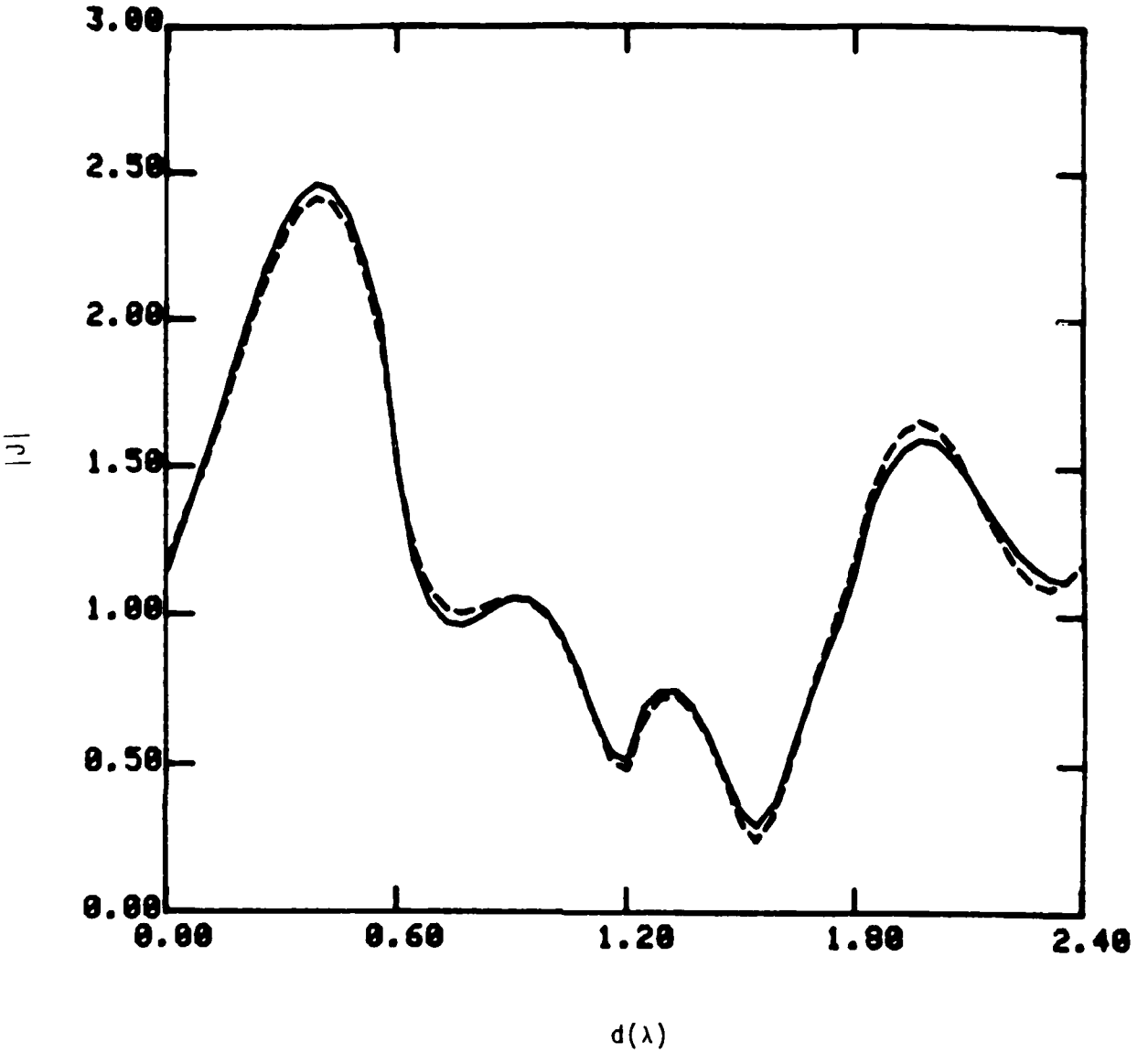

Figure 16. Magnitude of current on cylinder
$W = 0.6\lambda$, $\alpha = 65^0$
——— MM
- - - - - - - - - Iteration Method

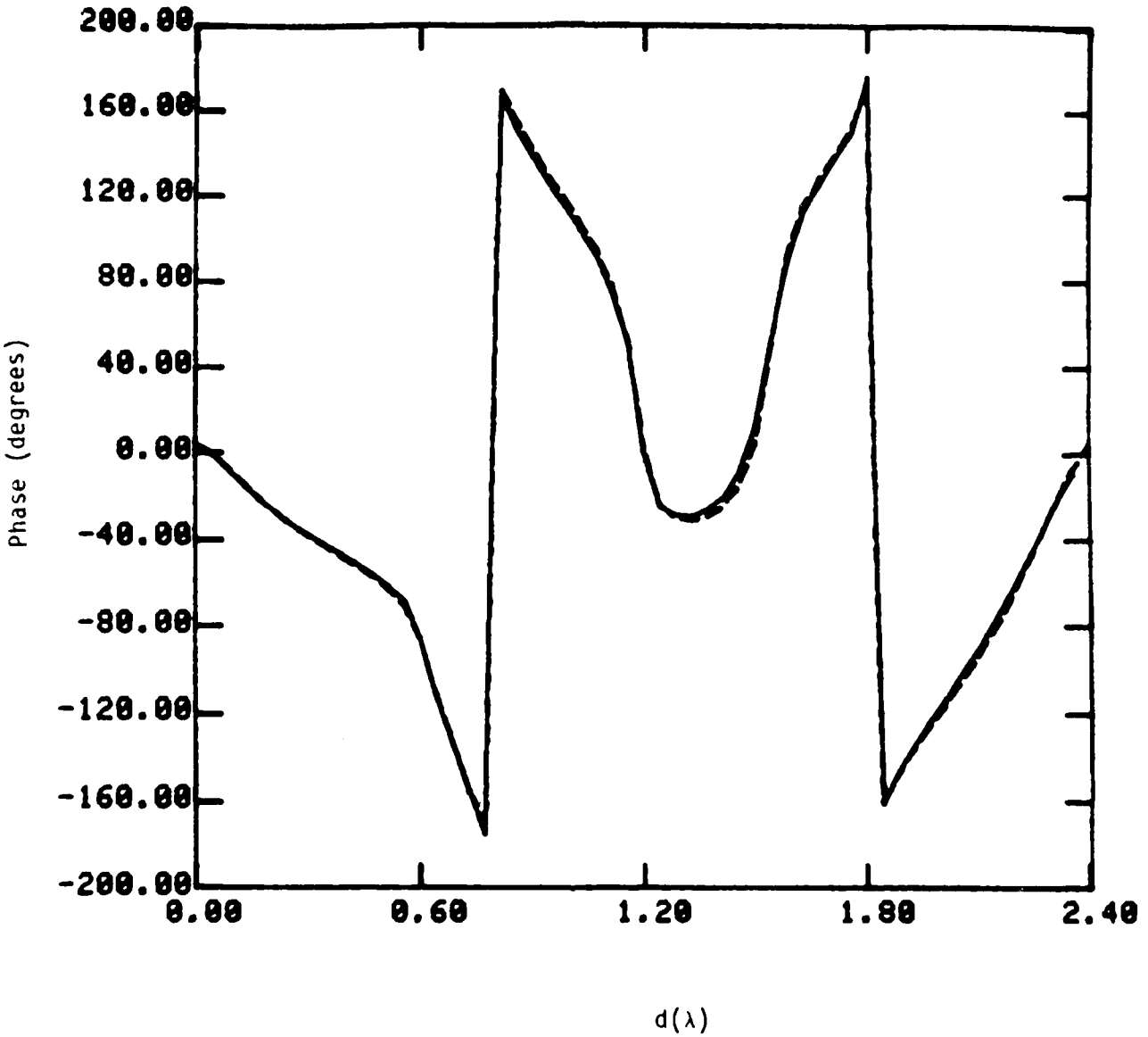

Figure 17. Phase of current on cylinder
$W = 0.6\lambda$, $\alpha = 65^0$
_____ MM
- - - - - - - - - Iteration Method

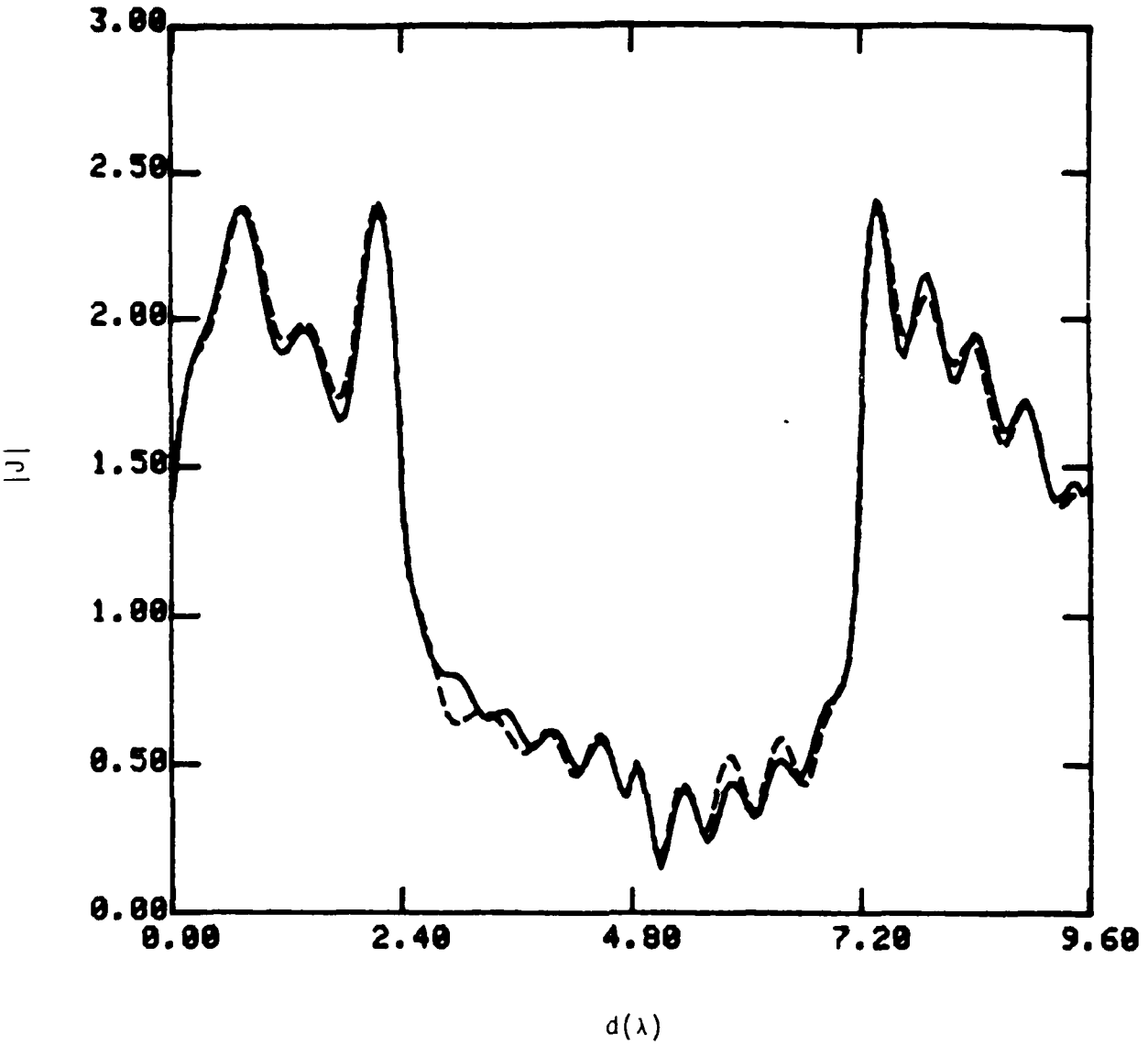

Figure 18. Magnitude of current on cylinder
W = 2.4λ, α = 65^0
_____ MM
- - - - - - - - - Iteration Method

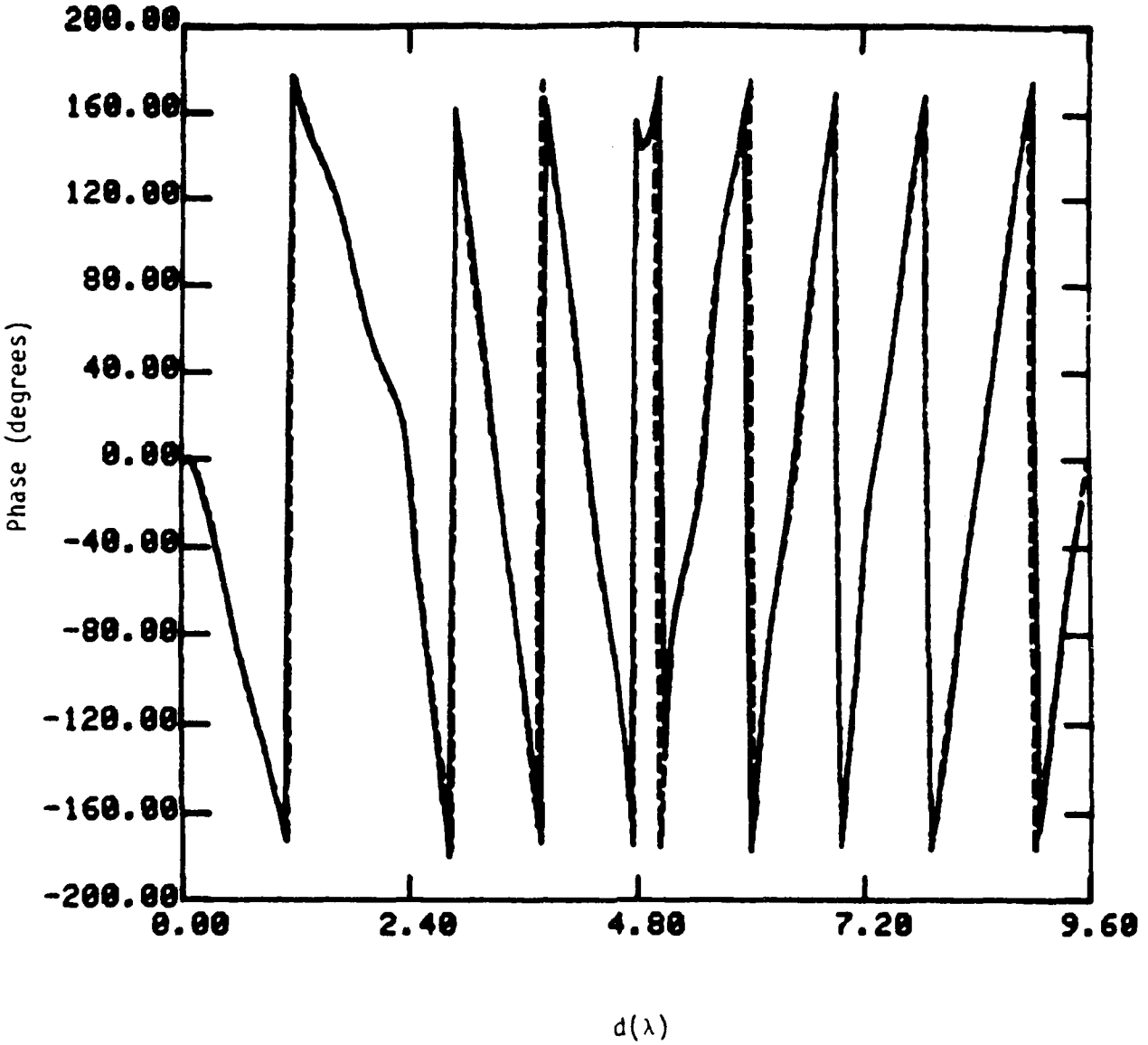

Figure 19. Phase of current on cylinder
$W = 2.4\lambda$, $\alpha = 65°$
_____ MM
- - - - - - - - - - Iteration Method

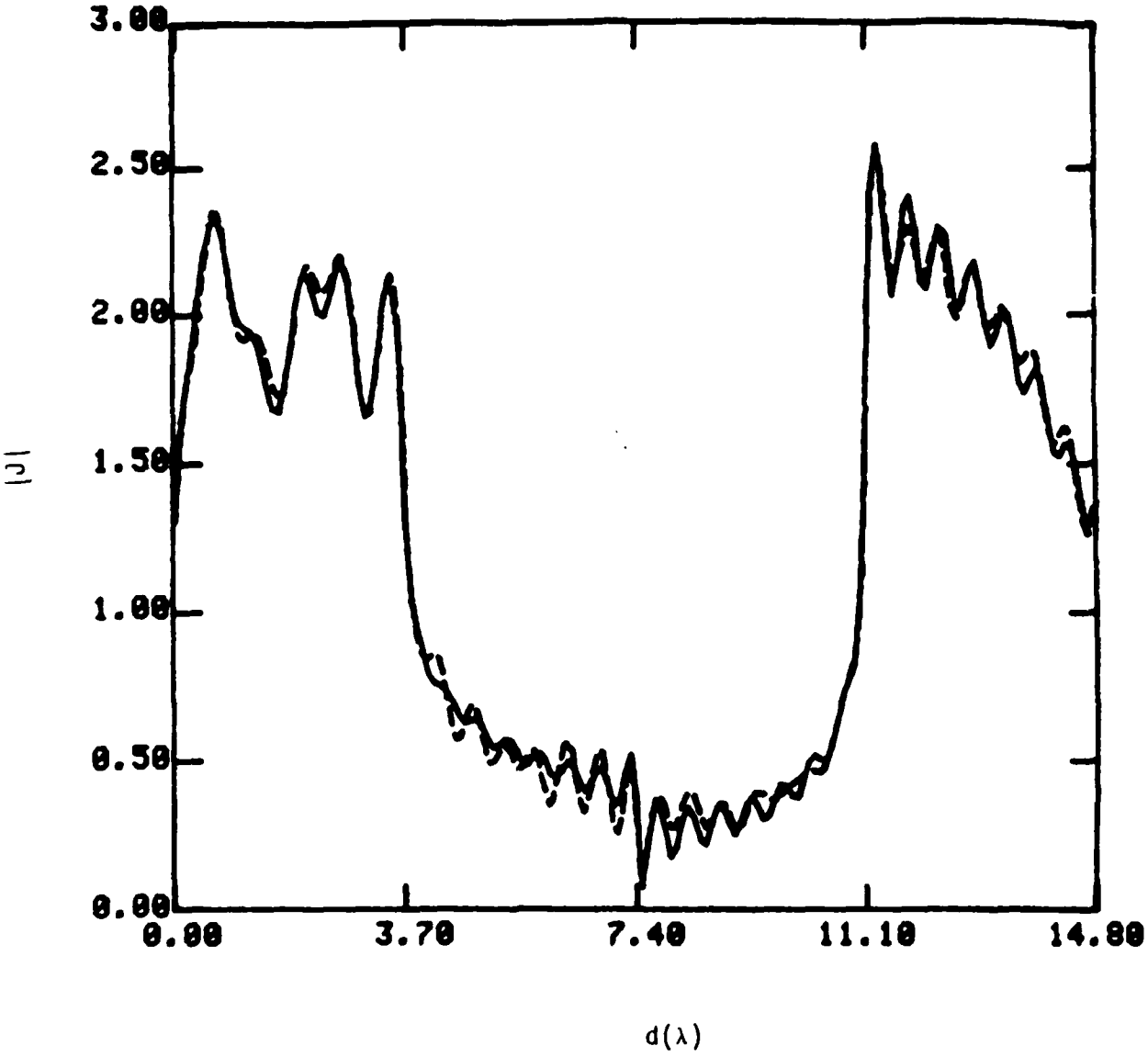

Figure 20. Magnitude of current on cylinder
W = 3.7λ, α = 65°
_____ MM
- - - - - - - - - - Iteration Method

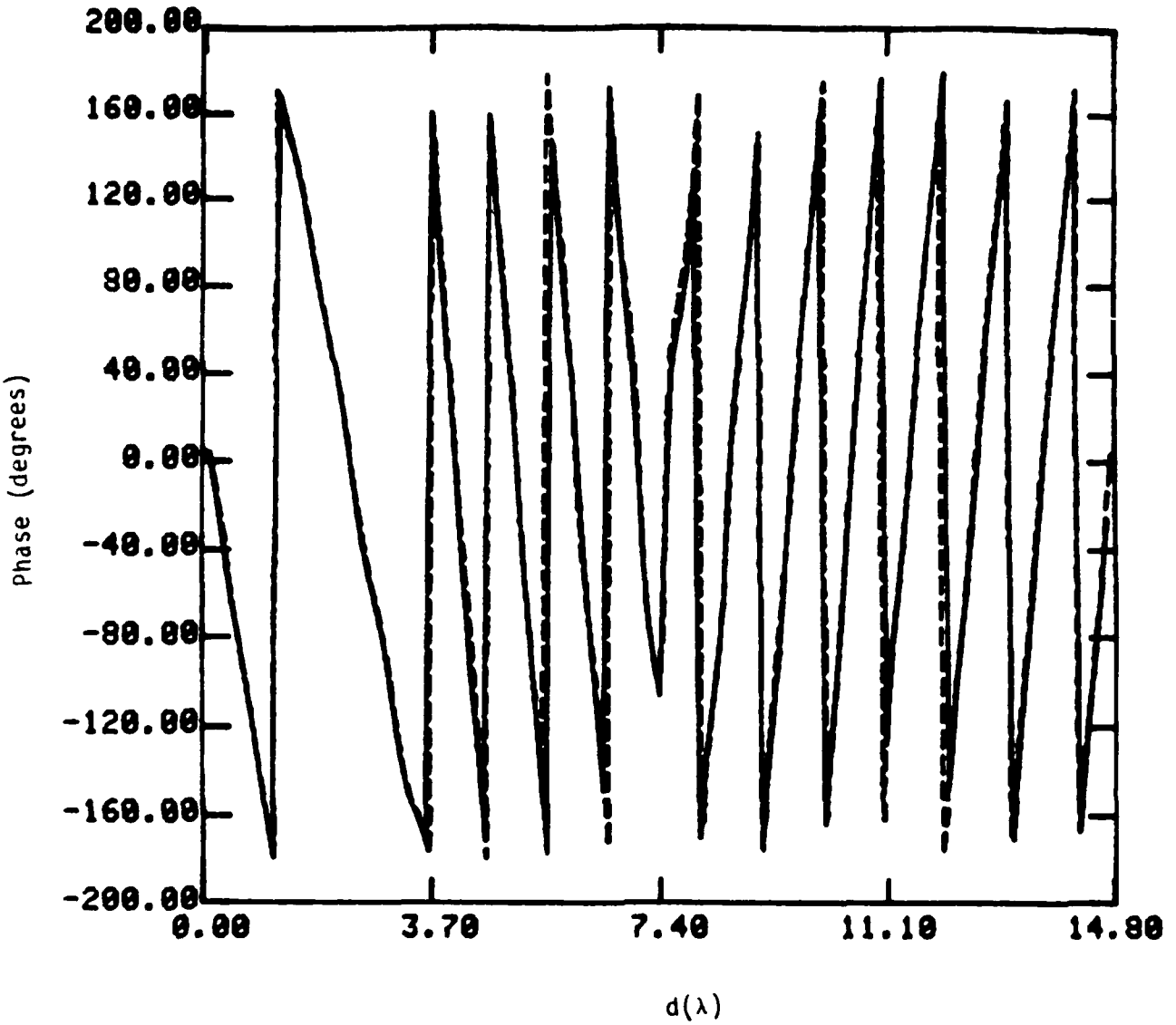

Figure 21. Phase of current on cylinder
$W = 3.7\lambda$, $\alpha = 65^0$
——— MM
- - - - - - - - - Iteration

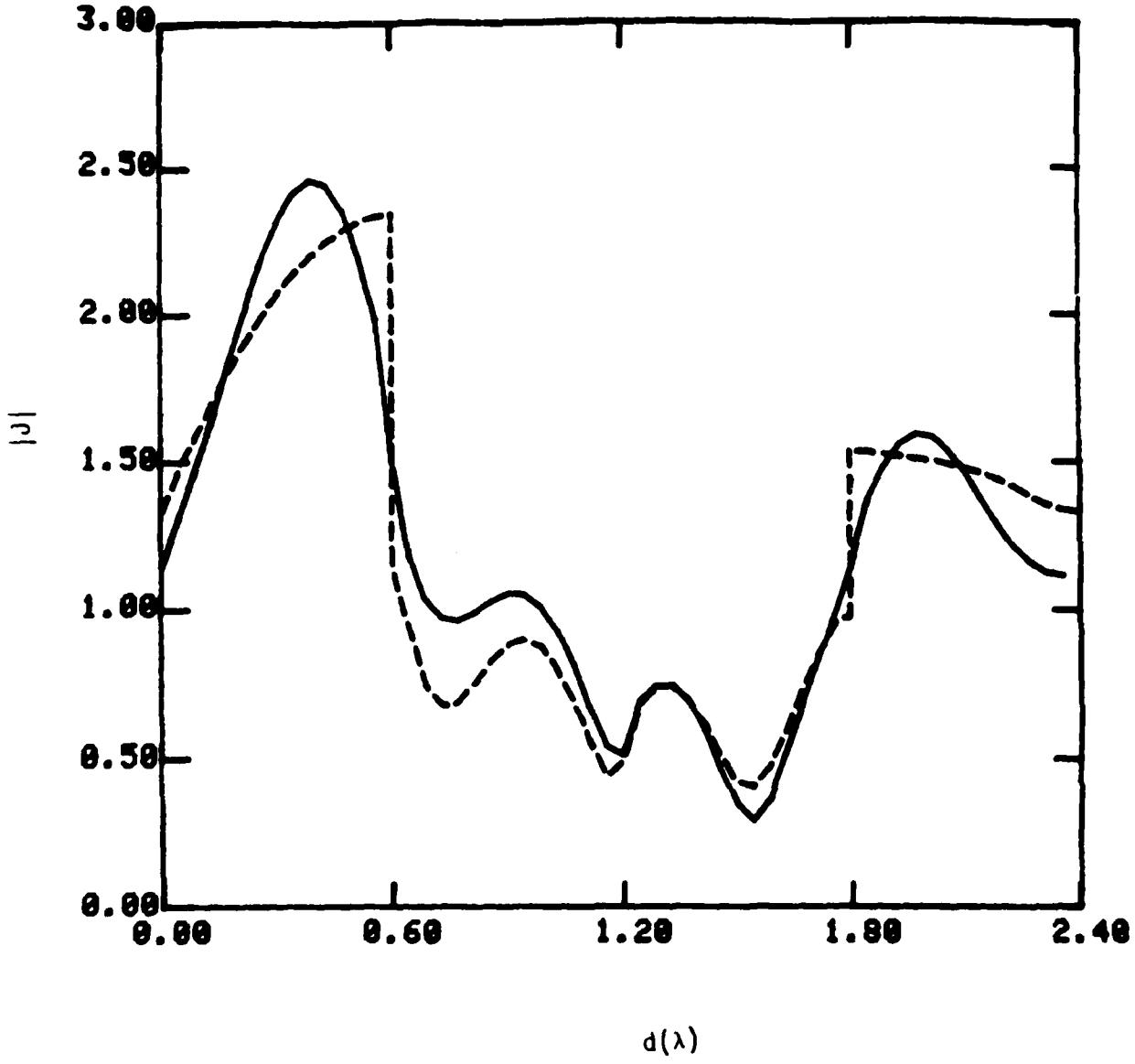

Figure 22. Magnitude of optics current on cylinder
W = 0.6λ, α = 65°
_____ MM
- - - - - - - - - - Optics current

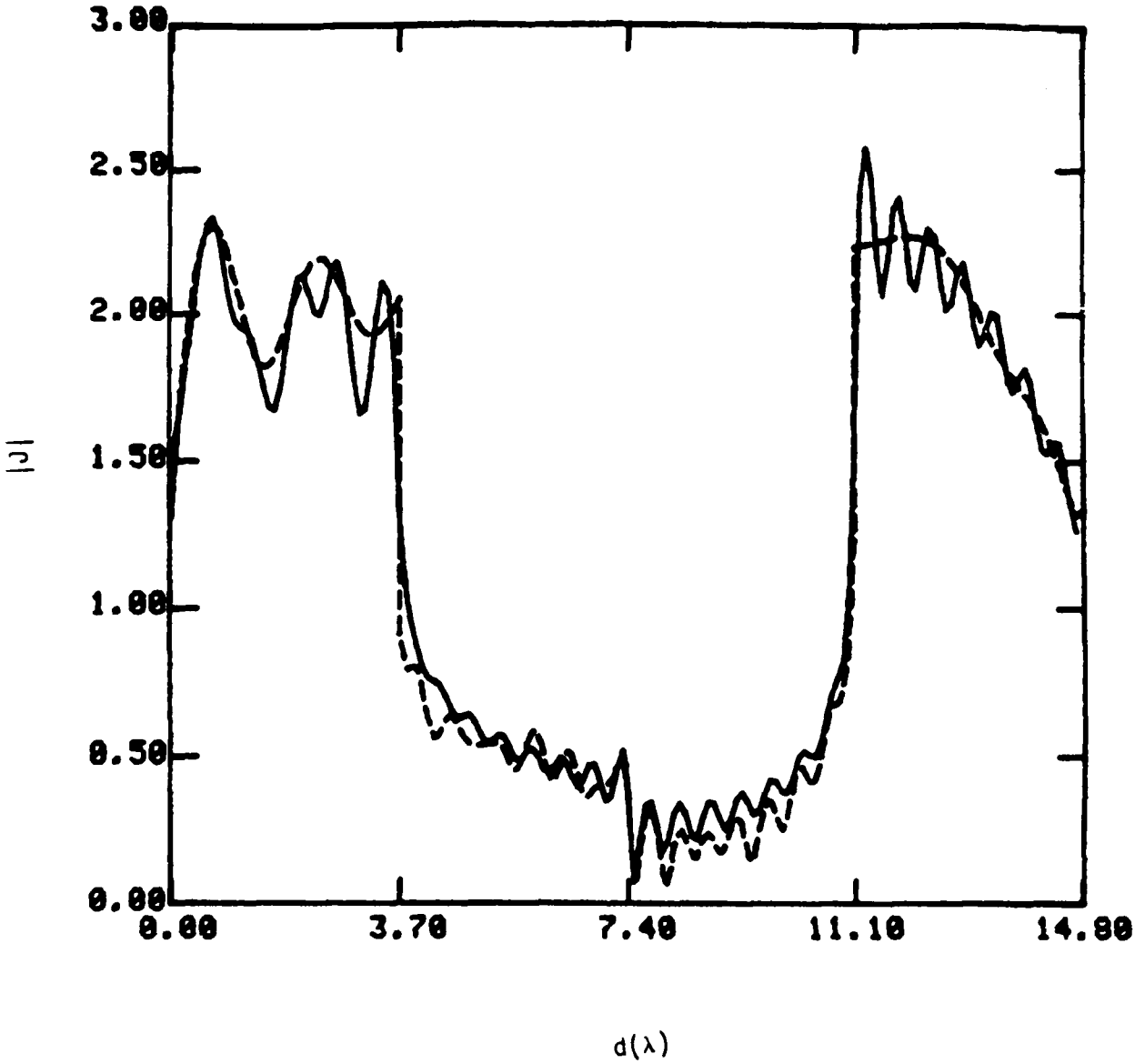

Figure 23. Magnitude of optics current on cylinder
W = 3.7λ, α = 65°
_____ MM
- - - - - - - - - - Optics current

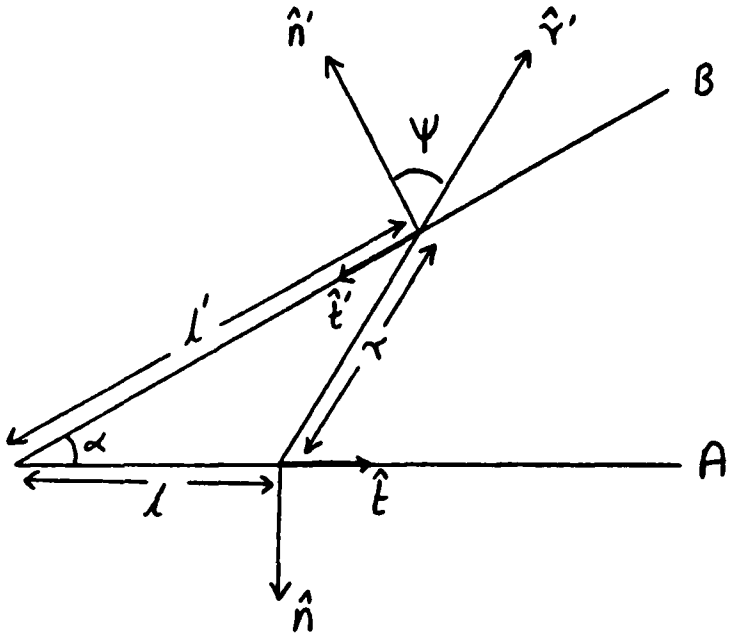

Figure 24. Geometry and definitions for edge current calculation

MISSION
of
Rome Air Development Center

RADC plans and executes research, development, test and selected acquisition programs in support of Command, Control Communications and Intelligence (C^3I) activities. Technical and engineering support within areas of technical competence is provided to ESD Program Offices (POs) and other ESD elements. The principal technical mission areas are communications, electromagnetic guidance and control, surveillance of ground and aerospace objects, intelligence data collection and handling, information system technology, solid state sciences, electromagnetics and electronic reliability, maintainability and compatibility.

Printed by
United States Air Force
Hanscom AFB, Mass. 01731

END

FILMED

3-85

DTIC